

Long-term validation of MIPAS ESA operational products using MIPAS-B measurements

Gerald Wetzel¹, Michael Höpfner¹, Hermann Oelhaf¹, Felix Friedl-Vallon¹, Anne Kleinert¹, Guido Maucher¹, Miriam Sinnhuber¹, Janna Abalichin², Angelika Dehn³, and Piera Raspollini⁴

5 ¹Karlsruhe Institute of Technology, Institute of Meteorology and Climate Research, Karlsruhe, Germany

²Freie Universität Berlin, Institute of Meteorology, Berlin, Germany

³European Space Agency (ESA-ESRIN), Frascati, Italy

⁴Istituto di Fisica Applicata “N. Carrara” (IFAC) del Consiglio Nazionale delle Ricerche (CNR), Firenze, Italy

Correspondence to: Gerald Wetzel (gerald.wetzel@kit.edu)

10

Abstract

The Michelson Interferometer for Passive Atmospheric Sounding (MIPAS) was a limb-viewing infrared Fourier transform spectrometer that operated from 2002 to 2012 aboard the Environmental Satellite (ENVISAT). The final re-processing of the full MIPAS mission Level
15 2 data was performed with the ESA operational version 8 (v8) processor. This MIPAS data set not only includes retrieval results of pressure-temperature and the standard species H₂O, O₃, HNO₃, CH₄, N₂O, and NO₂, but also vertical profiles of volume mixing ratios of the more difficult to retrieve molecules N₂O₅, ClONO₂, CFC-11, CFC-12 (included since v6 processing), HCFC-22, CCl₄, CF₄, COF₂, and HCN (included since v7 processing). Finally, vertical profiles
20 of the species C₂H₂, C₂H₆, COCl₂, OCS, CH₃Cl, and HDO were additionally retrieved by the v8 processor.

The balloon-borne limb-emission sounder MIPAS-B was a precursor of the MIPAS satellite instrument. Several flights with MIPAS-B have been carried out during the 10 years operational phase of ENVISAT at different latitudes and seasons, including both operational periods **when**
25 MIPAS measured with full spectral resolution (FR mode) and with optimized spectral resolution (OR mode). All MIPAS operational products (except HDO) were compared to results inferred from dedicated validation limb sequences of MIPAS-B. To enhance the statistics of vertical profile comparisons, a trajectory match method has been applied to search for MIPAS coincidences along 2-day forward/backward trajectories running from the MIPAS-B
30 measurement geolocations. This study gives an overview of the validation results based on the

ESA operational v8 data comprising the MIPAS FR and OR observation periods. This includes an assessment of the data agreement of both sensors, taking into account the combined errors of the instruments. The difference between retrieved temperature profiles of both MIPAS instruments generally stays within ± 2 K in the stratosphere. For most gases, namely H₂O, O₃, HNO₃, CH₄, N₂O, NO₂, N₂O₅, ClONO₂, CFC-11, CFC-12, HCFC-22, CCl₄, CF₄, COF₂, and HCN we find a 5-20 % level of agreement of the retrieved vertical profiles of both MIPAS instruments in the lower stratosphere. For the species C₂H₂, C₂H₆, COCl₂, OCS, and CH₃Cl, however, larger differences (within 20-50 %) appear in this altitude range.

40 1 Introduction

Satellite measurements of stratospheric trace gases are essential for monitoring the distribution and trend of these species on a global scale (Hegglin et al., 2021). The Environmental Satellite (ENVISAT) of the European Space Agency (ESA) operated between 2002 and 2012. The Michelson Interferometer for Passive Atmospheric Sounding (MIPAS; Fischer et al., 2008) was one of three chemistry instruments aboard ENVISAT, besides the Scanning Imaging Absorption Spectrometer for Atmospheric Chartography (SCIAMACHY; Bovensmann et al., 1999) and the Global Ozone Monitoring by Occultation of Stars (GOMOS) instrument (Bertaux et al., 1991). Validating instruments like MIPAS for the purpose of assessing measurement accuracy is an essential task. Stratospheric measurements with balloon instruments like MIPAS-B are particularly suitable to reach this goal since these instruments are able to sound the atmosphere with high vertical resolution (e.g. Wetzel et al., 2006; Cortesi et al., 2007; Ridolfi et al., 2007; Wang et al., 2007; Wetzel et al., 2007; Renard et al., 2008; Wetzel et al., 2008; Payan et al., 2009; Zhang et al., 2010; Sagawa et al., 2013; Wetzel et al., 2013a). The main logistical requirement that the satellite and the validating balloon instruments observe the same air masses has to be considered carefully when performing balloon campaigns. Two principal comparison methods are common: (1) direct matches where the balloon instrument measures at the same time and location where the satellite observation takes place and (2) trajectory matches where forward and backward trajectories are calculated from the balloon measurement geolocation to search for appropriate satellite overpasses. Along with (1) and (2), there is a dynamical approach using potential vorticity and potential temperature field as suggested by Manney et al. (2001). Several flights with the balloon version of MIPAS (Friedl-Vallon et al., 2004) were carried out during the operational time of ENVISAT. This study

presents an overview of 10 years of MIPAS observations based on the recent ESA processor version 8 (v8; released in 2021; ESA, 2021; Dinelli et al., 2021) and provides the evaluation of the long-term performance of MIPAS covering the complete set of atmospheric parameters (except HDO) that have been processed with the newest operational data version. In the following sections, validation activities, data analysis and validation results are described in detail.

2 Instruments and data analysis

2.1 MIPAS operations and data version

The limb-viewing Fourier transform spectrometer MIPAS on ENVISAT (hereinafter also referred to as MIPAS-E to better distinguish from the balloon instrument MIPAS-B) has been designed to operate in the mid-infrared spectral region covering five spectral bands between 685 and 2410 cm^{-1} with a maximum optical path difference (MOPD) of 20 cm, equivalent to an unapodized full spectral resolution of 0.025 cm^{-1} (Fischer et al., 2008). The vertical instantaneous field of view (IFOV) was about 3 km. ENVISAT was launched into its sun-synchronous orbit by ESA on 1 March 2002 with 14.3 orbits/day and an Equator crossing local solar time of 10:00 (descending node). After the commissioning phase, MIPAS-E was run predominantly in its nominal measurement mode with full spectral resolution (called FR mode) from July 2002 until the end of March 2004. During each orbit, approximately 72 limb scans covering tangent altitudes between 6 and 68 km were recorded (in steps of 3 km up to 42 km, and at 47, 52, 60, and 68 km) in the FR mode. The majority of validation studies based on correlative measurements published so far were addressing MIPAS-E data recorded during this first time period. These measurements were originally reprocessed by the ESA Instrument Processing Facilities (IPF) v4.1 and v4.2, based on the Optimized Retrieval Model (ORM) code described in Ridolfi et al. (2000) and Raspollini et al. (2006), and covered pressure-temperature and the six constituents O_3 , H_2O , CH_4 , N_2O , HNO_3 , and NO_2 . The validation studies addressed these parameters and constituents: pressure-temperature (Ridolfi et al., 2007), O_3 (Cortesi et al., 2007), HNO_3 (Wang et al., 2007), NO_2 (Wetzel et al., 2007), N_2O and CH_4 (Payan et al., 2009), and H_2O (Wetzel et al., 2013a).

After an increasing frequency of problems with the interferometer drive system in late 2003 and beginning of 2004 and upon subsequent detailed investigations, it was decided to suspend

the nominal operations from March 2004 onwards for detailed investigations. From January
95 2005 onwards, the instrument was back in operation but at reduced MOPD (41 % of nominal)
while maintaining the interferogram scan speed. During data processing, the interferograms
were truncated to 8 cm MOPD, resulting in an unapodized spectral resolution of 0.0625 cm^{-1} .
The shorter acquisition time per interferogram led to the benefit of an equivalent improvement
in the vertical and horizontal (along-track) sampling (nominal tangent altitudes: 6, 7.5, 9, 10.5,
100 12, 13.5, 15, 16.5, 18, 19.5, 21, 23, 25, 27, 29, 31, 34, 37, 40, 43, 46, 50, 54, 58, 62, 66, and 70
km.) The duty cycle of this so-called optimized resolution (OR) mode (optimized in terms of a
trade-off between spectral and spatial resolution considering instrument operation safety
aspects) was steadily increased from 30 % in January 2005 to 100 % from December 2007 on.
MIPAS-E was successfully operated with this full duty cycle in the OR mode until 8 April
105 2012, when an ENVISAT anomaly occurred, resulting in the loss of communication between
ground and satellite and the end of MIPAS-E observations (ESA, 2012). Details of the
characteristics of the two MIPAS-E mission phases (FR and OR modes) in terms of instrument
settings and atmospheric sampling are described in Raspollini et al. (2013) and Dinelli et al.
(2021).

110 The coarser spectral but finer spatial sampling of MIPAS-E since 2005 along with the need for
near real time analysis demanded adaptations in the calibration scheme and the processing
codes. This was realized in ESA Level (L) 2 processor version (v) 6 and explained by Raspollini
et al. (2013), which also provides the diagnostics of the products including the error budgets as
estimated by Dudhia et al. (2002). The whole MIPAS-E data set covering almost 10 years of
115 observations was re-processed with v6, v7, and v8. In addition, the number of retrieved
constituents was extended to ClONO_2 , N_2O_5 , CFC-11, and CFC-12 in ESA version 6.

ESA version 7 data (released in 2015) also includes the species HCN, HCFC-22, CF_4 , COF_2 ,
and CCl_4 . The ESA L1v8/L2v8 diagnostic data set (DDS) version was released in June 2018
followed by the L1v8/L2v8 full mission (FM) data in June 2019. The new v8 data release (ESA,
120 2021; Dinelli et al., 2021; Raspollini et al., 2022) comprises the additional molecules C_2H_2 ,
 C_2H_6 , COCl_2 , OCS, CH_3Cl , and HDO. For the final ESA reprocessing of MIPAS-E data,
numerous improvements were implemented in the L2 processor Optimised Retrieval Model
(ORM) version 8.22 (v8) and its auxiliary data including an update of the spectroscopic data
used (Raspollini et al., 2022). An exemplary overview on spectral regions used for the
125 operational retrievals together with typical errors (winter, OR mode) is given in Table 1. All

molecules except HDO have been validated by comparison with observations of the MIPAS balloon instrument.

2.2 MIPAS-B data set

130 The balloon-borne limb-emission sounder MIPAS-B can be regarded as a precursor of the MIPAS satellite instrument (Friedl-Vallon et al., 2004). Hence, a number of specifications like spectral resolution and spectral coverage are similar. The unapodized full spectral resolution is 0.0345 cm^{-1} , which is slightly coarser than the FR mode resolution but higher than the OR mode resolution. However, for essential parameters the MIPAS-B performance is superior, in terms of NESR (Noise Equivalent Spectral Radiance) and line of sight (LOS) stabilization. The LOS
135 is stabilized using an inertial navigation system supplemented with an additional star reference system which leads to an after all knowledge of the tangent altitude of better than 50 m at the 1σ confidence limit (Wetzel et al., 2010). The MIPAS-B NESR is further improved by averaging multiple spectra recorded at the same elevation angle. The general data processing from interferograms to calibrated spectra including instrument characterization is described in
140 Friedl-Vallon et al. (2004) and references therein.

MIPAS-B measurements were recorded typically at a 1.5 km vertical tangent altitude grid. Retrieval calculations of temperature and atmospheric trace species were performed at a 1 km grid with a Gauss-Newton iterative method (Rodgers, 2000) using analytical derivative spectra calculated by the Karlsruhe Optimized and Precise Radiative transfer Algorithm (KOPRA;
145 Stiller et al., 2002; Höpfner et al., 2002). To avoid retrieval instabilities due to oversampling of vertical grid points, a regularization approach according to the method described by Tikhonov (1963) and Phillips (1962) constraining with respect to the first derivative of the a priori profile was adopted. The resulting vertical resolution is typically between 2 and 5 km for the analysed atmospheric parameters and is therefore comparable to or slightly better than the vertical
150 resolution of the MIPAS satellite instrument. Table 2 gives an overview of the spectral windows used for the MIPAS-B target parameter retrievals. Different spectral microwindows within mostly the same molecular bands were used for the MIPAS-E data analysis (Dinelli et al., 2021). Spectroscopic parameters for the calculation of the infrared emission spectra originate from the high-resolution transmission (HITRAN) molecular absorption database (Rothman et al., 2009) and a MIPAS-E dedicated spectroscopic database (Raspollini et al., 2022). For heavy
155 molecules like CFC-11, CFC-12, HCFC-22, CCl_4 , and CF_4 , new and improved infrared

absorption cross sections (Harrison, 2015; Harrison, 2016; Harrison et al., 2017) were used for the calculation of radiative transfer (consistent **with** the MIPAS-E retrieval).

160 The MIPAS-B error budget includes random noise as well as covariance effects of the fitted parameters, temperature errors, pointing inaccuracies, errors of non-simultaneously fitted interfering species, and spectroscopic data errors (1σ). For further details on the MIPAS-B data analysis and error estimation, see Wetzel et al. (2012; 2015) and references therein. An overview of typical errors for the atmospheric parameter **retrievals** is given in Table 2.

2.3 Validation approach

165 A number of MIPAS balloon flights have been carried out as part of the validation program of the chemistry instruments aboard ENVISAT. Most of the MIPAS-B data used here, however, were obtained during flights that were done in the framework of various scientific projects. MIPAS-B had a sophisticated pointing system so that the full freedom of a balloon-borne limb emission sounder in terms of observation time, viewing direction and sampling strategy could
170 be used to get the best possible coincidence in time and space with the satellite overpass even during balloon flights that were not primarily dedicated to satellite validation. If compliant with the scientific goal of the mission and the weather conditions, the strategy was to launch the balloon in due time before an ENVISAT overpass and to optimize the azimuthal viewing direction and the vertical sampling at the time of the overpass. Except for two flights, a
175 coincidence in space and time between both sensors could be achieved such that vertical profiles of both instruments can be directly compared. An overview of the MIPAS balloon flights used in this study is given in Table 3.

To enhance the statistics of profile comparisons, diabatic 2-day forward and backward trajectories were calculated by the Free University of Berlin using a trajectory model (Naujokat
180 and Grunow, 2003; Grunow, 2009). The trajectories are based on European Centre for Medium-Range Weather Forecasts (ECMWF) $1.25^\circ \times 1.25^\circ$ analyses and start at different altitudes at the geolocation of the balloon observation to search for a coincidence with the satellite measurement along the trajectory path within a match radius of 1 h and 500 km. Temperature and volume mixing ratio (VMR) of the satellite match have been interpolated to the trajectory
185 match altitude such that these values can be directly compared to the MIPAS-B data at the trajectory start point altitude. Altitude differences between the trajectory start and match point

have to be taken into account in the case of temperature by means of an adiabatic correction. The handling of the diurnal variation of photochemically active species is discussed below.

The primary vertical coordinate of MIPAS-E is pressure whereas for MIPAS-B it is altitude.

190 For all intercomparisons shown in this study, **MIPAS-E pressure altitudes were logarithmically interpolated to the MIPAS-B hydrostatic pressure levels. Hence**, vertical profiles refer to the MIPAS-B pressure-altitude grid. Differences between measured quantities of MIPAS-E and the validation instrument MIPAS-B are expressed in absolute and relative units. The mean difference Δx_{mean} for N profile pairs of compared observations is given as:

$$195 \quad \Delta x_{mean} = \frac{1}{N} \sum_{n=1}^N (x_{E,n} - x_{B,n}), \quad (1)$$

where x_E and x_B are data values of MIPAS-E and MIPAS-B at one altitude level respectively. The mean relative difference $\Delta x_{mean,rel}$ of a number of profile pairs is calculated by dividing the mean absolute difference by the mean profile value of the reference instrument MIPAS-B:

$$\Delta x_{mean,rel} = \frac{\Delta x_{mean}}{\frac{1}{N} \sum_{n=1}^N x_{B,n}} \cdot 100\% . \quad (2)$$

200 Differences are displayed together with the combined errors σ_{comb} of both instruments, which are defined as:

$$\sigma_{comb} = \sqrt{\sigma_E^2 + \sigma_B^2}, \quad (3)$$

where σ_E and σ_B are the precision, systematic or total errors of MIPAS-E and MIPAS-B, respectively. **All errors discussed here refer to the 1σ confidence limit.**

205 Precision errors characterize the reproducibility of a measurement and correspond, in general, to random noise errors. Systematic errors used for the MIPAS-E data analysis have been assessed in corresponding studies (Dudhia et al., 2002; Raspollini et al., 2013; Dinelli et al., 2021). The uncertainty of the calculated mean difference (standard error of the mean, SEM) is given by $\sigma/N^{0.5}$ where σ is the standard deviation (SD). A bias between both instruments is considered significant if the SEM is smaller than the bias itself. The comparison between the VMR difference and the combined systematic error (for statistical comparisons) or total error (for single comparisons) is appropriate to identify unexplained **relative** biases in the MIPAS-E measurements when they exceed these combined error limits. Since the vertical resolution of

the atmospheric parameter profiles of both instruments is of comparable magnitude, a
215 smoothing by averaging kernels has not been applied to the observed profiles. The method
described above was performed for each individual balloon flight comparison. A mean
difference (with mean statistical parameters) for all flights was calculated by weighting the
mean result of each individual flight equally.

Photochemically reactive gases like NO_2 and N_2O_5 , and, to a lesser extent, ClONO_2 (mainly in
220 the Tropics) undergo a diurnal variation with changing solar zenith angle (SZA). For these
gases, a photochemical correction taking into account differences in the SZA between the
measurements of both sensors has been applied. The molecule NO_2 exhibits the most
pronounced temporal variation. The partitioning of NO , NO_2 , and N_2O_5 within the NO_y family
depends strongly on the SZA due to the rapid **daytime** photolysis of NO_2 and the slower
225 photolysis of N_2O_5 . **At sunset, NO is rapidly converted to NO_2 mainly via the reaction with O_3 .
During the night, NO_2 is gradually decomposed to form N_2O_5 .** A 1-dimensional model (Bracher
et al., 2005) was constrained with NO_y species measured by MIPAS-B and initialized with the
output of a global 2-dimensional model (Sinnhuber et al., 2003) to calculate SZA correction
factors for the MIPAS-E data.

230

3 Intercomparison results

In the following subsections we discuss the validation for all quantities delivered operationally
by ESA's L1v8/L2v8 FM processor on the basis of collocated MIPAS-B observations. Only
MIPAS satellite data that have passed the a posteriori quality check (mainly retrieval
235 convergence and size of maximum error, **for details see Raspollini et al., 2022**) were used for
the intercomparison. The analysis of all compared vertical profiles is regarded as evaluation
with the highest statistical evidence. Trajectory matches are based on diabatic 2-day forward
and backward trajectories with a collocation criterion of 1 h and 500 km as described in section
2.

240 Since the balloon flights were performed between 2003 and 2011, they cover almost the full
ENVISAT operational period of 2002 to 2012, i.e., both MIPAS-E mission phases (FR and OR
modes) with distinctly different instrument settings. A compilation of all vertical profiles of
temperature and 20 species retrieved from MIPAS-B spectra is given in Fig. 1. We performed
the intercomparison analysis separately not only for different climatological regions but also
245 for the periods 2002-2004 and 2005-2012. The following intercomparison is focused on these

two periods when MIPAS-E was operated in the FR and OR mode, respectively. An overview of the most important findings of this intercomparison is listed in Table 4. A comprehensive MIPAS-E quality readme file not only including the validation results related to MIPAS-B, but in addition ground-based, ACE-FTS (Atmospheric Chemistry Experiment – Fourier Transform Spectrometer), lidar, radiosonde, and ozone sonde validation results was published by Raspollini et al. (2020).

3.1 Temperature

Apart from its relevance as primary atmospheric state parameter, the quality of temperature data is essential in the atmospheric emission limb sounding since temperature profiles generally are retrieved prior to the trace gas retrievals. Hence, temperature errors propagate in subsequent retrievals of trace constituents. Our study shows that above about 11 km the mean differences between MIPAS-B and MIPAS-E are within ± 2 K and within the combined systematic errors, although the standard deviations exceed the expected precision (see Fig. 2). In the lowermost stratosphere and around the tropopause, MIPAS-E exhibits a positive bias with respect to the balloon instrument in the OR mode and the Tropics. Differences between both sensors are comparable to the findings of a comprehensive temperature validation study by Ridolfi et al. (2007) that was addressing the FR mode period only using version 4.61 and 4.62 data. However, the large temperature differences between MIPAS-E and MIPAS-B in the tropical troposphere are not seen in a comparison to groundbased data (Hubert et al., 2020). A possible reason for this difference between both MIPAS sensors could be an inaccuracy in the altitude assignment (the tropopause altitude difference between both MIPAS instruments is up to 1 km), which has a particularly strong effect in combination with the strong vertical temperature gradient in the troposphere.

3.2 H₂O

In view of the ongoing debates on long-term trends of water vapour (e.g. Dessler et al., 2014; Lossow et al., 2018; Khosrawi et al., 2018), we carefully looked at the consistency of the validation results of the MIPAS-E FR phase with respect to the MIPAS-E OR phase. Figure 3 presents the intercomparison results. FR and OR mode comparisons show different vertical shapes of the differences between MIPAS-E and MIPAS-B. For a molecule like H₂O with strong vertical VMR gradients, this might be at least partly explained by the fact that the MIPAS-E vertical resolution is somewhat higher in the OR mode compared to the FR phase

(together with a larger retrieval error in the OR mode with respect to the FR phase) as shown by Dinelli et al. (2021). In the lowermost stratosphere and upper troposphere, MIPAS-E significantly overestimates H₂O and exceeds the combined systematic error bars around 15 km in the OR mode. This general behaviour remains also in the statistical analysis of all collocations. In the middle and upper stratosphere, a positive bias of MIPAS-E against MIPAS-B (increasing with altitude in the FR period) of 5-20 % is visible, although the errors stay (except at 37 km) within the predicted error budget. These findings are in line with the conclusions drawn from a comprehensive validation study of MIPAS-E (version 4.61) phase one (FR mode) observations by Wetzell et al. (2013a). The differences found in the FR and OR modes also agree with the discrepancies seen in the Stratosphere-troposphere Processes and their Role in Climate (SPARC) Data Initiative where non-operational MIPAS-E data (Clarmann et al., 2009) were compared to the multi-instrument mean of satellite sensors (Hegglin et al., 2021). No major differences were seen between MIPAS-E v7 (as used in the SPARC comparisons) and v8 data (Lossow et al., 2019). The pronounced deviation between both MIPAS sensors in the tropical troposphere may possibly be explained by an inaccuracy in the altitude assignment (the hygropause altitude difference between both MIPAS instruments is up to 1 km) in combination with the strong vertical H₂O gradient in this altitude region.

3.3 O₃

The monitoring of the expected recovery of the stratospheric ozone layer, and in particular the Antarctic ozone hole, still remains of great scientific interest (e.g. Carpenter et al., 2014; Dhomse et al., 2019). Hence, ozone was one of the key species during the ENVISAT mission. Comparisons based on the full statistics over all collocations show an agreement between the satellite and the balloon data within ± 10 % above 15 km for this mainly stratospheric species (see Fig. 4). For most of the stratosphere (17-37 km), the mean relative difference between the data sets is always within ± 5 %. Furthermore, differences of the combined FR plus OR mode are within the combined systematic error. Degradation in the quality of the agreement is observed in the lower stratosphere and upper troposphere, with deviations up to about 20 % in both observation periods. Generally, the statistical agreement between the two data sets is comparable to that reported by Cortesi et al. (2007) for the FR mode phase (v4.61/v4.62) as deduced from an extensive study using various kinds of correlative data.

3.4 HNO₃

HNO₃ is an important stratospheric nitrogen reservoir species (see e.g. Brasseur and Solomon, 2005). VMR difference profiles of this trace gas are presented in Fig. 5. MIPAS-E tends to overestimate the HNO₃ abundance when compared to MIPAS-B below about 27 km. This bias is most prominent in the OR mode data between 19 and 26 km around the altitude of the VMR maximum of the HNO₃ profile. Biases are typically in the order of 5-20 % in relative units and in line with the numbers reported by Wang et al. (2007) referring to the FR period (v4.61/v4.62). Positive biases of comparable magnitude between non-operational MIPAS-E data and the multi-instrument mean were also found at mid and high latitudes in the SPARC Data Initiative comparison (SPARC, 2017). Standard deviations clearly exceed the expected precision.

3.5 CH₄ and N₂O

These two species are long-lived tracers of similar lifetimes and are therefore correlated to each other (see e.g. Michelsen et al., 1998). Hence, they are discussed together in this study. Figures 6 and 7 present the results for these molecules based on the statistical trajectory analysis of all collocations available. Both species show a quite similar altitude-dependent behaviour of the mean difference in absolute and relative quantities while standard deviations exceed the expected precision. MIPAS-E tends to overestimate the abundance of both species in the stratosphere below about 35 km by 5-15 % (CH₄) and 10-20 % (N₂O), respectively. A similar positive bias has already been mentioned in the (FR mode, v4.61) validation study by Payan et al. (2009). A similar behaviour is found for non-operational products of other algorithms analysing MIPAS-E data in the SPARC Data Initiative comparison in the stratosphere and upper troposphere, especially in the FR mode period (SPARC, 2017). Somewhat larger positive deviations between both MIPAS instruments are visible in the Tropics around 30 km.

3.6 NO₂

NO₂ exhibits a strong diurnal variation in the stratosphere and is in photochemical equilibrium with NO and N₂O₅ (see e.g. Brasseur and Solomon, 2005). This needs to be taken into account when comparing NO₂ data sets of different SZA. For our study, a photochemical correction considering differences in the SZA between the measurements of both sensors has been applied as described in more detail in section 2. Figure 8 presents the statistical trajectory match analysis. It indicates a positive bias (up to 20 %, unexplained above 31 km) of MIPAS-E NO₂

in the FR period that is becoming increasingly significant from lower to higher altitudes. This is in line with the findings of the comprehensive NO₂ validation study (FR mode) reported by Wetzel et al. (2007) referring to v4.61 MIPAS-E data. In the OR period, the positive bias (above 27 km) between both sensors is smaller and amounts to about 10 %. Differences recognized during the SPARC Data Initiative are quite time-variable. However, differences between the MIPAS instruments as shown here stay within the standard deviation of the differences between non-operational MIPAS-E data and the multi-instrument mean of satellite sensors (SPARC, 2017).

3.7 Additional v6 products: N₂O₅, ClONO₂, CFC-11, and CFC-12

Starting with processor v6, four additional target species, namely N₂O₅, ClONO₂, CFC-11, and CFC-12, have been operationally processed by ESA. A first validation study of these species was carried out by Wetzel et al. (2013b).

N₂O₅ is a temporary reservoir of reactive nitrogen in the stratosphere and exhibits a prominent diurnal variation with maxima just before sunrise and minima just before sunset (see e.g. Brasseur and Solomon, 2005). The general agreement between MIPAS-E and MIPAS-B is within ±10 % between 24 and 34 km for the mean of all collocations (see Fig. 9). Below 24 km and above 34 km, mean differences exceed at least partly the systematic errors suggesting the need for a more careful use of the MIPAS-E N₂O₅ data for scientific studies in these altitude regimes. No significant bias is visible in the OR mode, but a small negative bias is obvious in the FR period. The validation results are in line with the v6 comparison study by Wetzel et al. (2013b).

ClONO₂ is a major reservoir of reactive chlorine in the stratosphere and is involved in heterogeneous chemistry in the context of ozone depletion at high latitudes (e.g. Clarmann and Johansson, 2018, and references therein). It undergoes diurnal variations at higher altitudes during periods of stronger illumination, therefore it had to be photochemically corrected there. Figure 10 presents the intercomparison results for all collocations. In the altitude region where ClONO₂ concentrations are most relevant, both data sets are consistent. Differences are within ±10 % between 17 and 34 km without a clear bias. Only at the upper and lower altitude edge of the comparisons, the mean differences exceed the combined systematic errors. However, standard deviations clearly exceed the expected precision. The v8 validation results are comparable to the outcome of the study performed by Wetzel et al. (2013b) referring to v6 data.

The gases CFC-11 (CCl_3F) and CFC-12 (CCl_2F_2) are rather long-lived chlorofluorocarbons (Ko and Dak Sze, 1982). Results are shown in Figs. 11 and 12, respectively. In the case of CFC-12, mean differences remain within the combined errors and are within $\pm 5\%$ (smaller than in previous versions, not shown in the plots) below 20 km. Above this altitude, a significant positive bias is visible (up to 32 km) and standard deviations exceed the expected precision. However, this bias is less pronounced than in the validation studies performed by Engel et al. (2016) and Wetzel et al. (2013b) that were based on observations in comparison to MIPAS-E v6 data. Deviations for CFC-11 are somewhat larger than for CFC-12, up to $\pm 10\%$ below 20 km. An increasing positive bias is obvious above this altitude level. However, CFC-11 differences between both MIPAS instruments are smaller compared to the differences shown in the previous validation study by Engel et al. (2016). The improvement in the quality of the CFC-11 v8 data set compared to v6 is also clearly seen if one considers previous comparisons to the MIPAS balloon observations (Wetzel et al., 2013b).

3.8 Additional v7 products: HCFC-22, CCl_4 , CF_4 , COF_2 , and HCN

Five more species have been operationally processed by the v7 algorithm. To date, an intercomparison study is only available for CCl_4 profiles (Valeri et al., 2017). It should be mentioned that these species are generally more difficult to retrieve than the gases described before. This holds also for the MIPAS-B retrieval, although these gases can be measured with higher accuracy (mainly due to lower spectral noise) compared to MIPAS-E. Hence, some unexplained features (exceeding combined systematic errors) in the VMR difference profiles are expected to occur more frequently when comparing these molecules.

HCFC-22 (CHClF_2) is a longer-lived hydrochlorofluorocarbon. Since HCFC-22 is often used as an alternative to the highly ozone-depleting CFC-11 and CFC-12, its tropospheric concentration is further increasing (e.g. Chirkov et al., 2016). Comparison results are depicted in Fig. 13. In the FR mode period, differences between both instruments remain within $\pm 10\%$ up to 26 km turning into a significant positive bias for MIPAS-E above this altitude. In the OR observation period, deviations stay within 10% for altitudes up to 28 km while a significant negative bias is visible in the MIPAS-E data above this altitude level. Standard deviations exceed the expected precision at higher altitudes (mainly OR phase).

The tropospheric mixing ratio of the longer-lived source gas CCl_4 is clearly decreasing since the beginning of the 1990s (Prinn et al., 2000). However, estimated sources and sinks of this

400 molecule are inconsistent with observations of its abundance (Carpenter et al., 2014). A significant negative bias shows up in the MIPAS-E CCl₄ data (full period) above 22 km (see Fig. 14), which is **close to** the combined systematic error limits. A significant positive bias is visible below 21 km during the OR phase. However, differences stay within $\pm 20\%$ up to about 22 km in both observation periods, which is in line with the deviations reported by Valeri et al. (2017) referring to v7 data.

405 The fluorocarbon CF₄ has an extremely long atmospheric lifetime of more than 50000 years and its atmospheric concentration is linearly increasing (Carpenter et al., 2014). Comparison results are shown in Fig. 15. **There is general agreement between both instruments between** 11 and 37 km (within $\pm 10\%$ in both observation periods). In the FR phase, a significant positive bias above 10 km is visible. In contrast, no clear bias is obvious in the OR period where
410 differences stay within $\pm 10\%$ at all altitudes. However, standard deviations exceed the expected precision in the OR phase.

The molecule COF₂ is a stratospheric reservoir species for fluorine (Harrison et al., 2014). The general profile shape (as measured by MIPAS-B) is reproduced by MIPAS-E (see Fig. 16). Stratospheric VMR differences stay within $\pm 10\%$ in the FR period and $\pm 20\%$ in the OR period.
415 No unexplained biases (in terms of combined systematic error bars) are evident.

HCN is mainly produced by biomass burning and hence considered as an almost unambiguous tracer for biomass burning events (e.g. Li et al., 2003). Differences are within $\pm 20\%$ below 34 km (see Fig. 17). A significant positive bias (more than 20 %) is evident in the MIPAS-E profiles observed in the FR mode period, **exceeding** the combined systematic error limits above
420 20 km. This pronounced bias is visible in each comparison of the three MIPAS-B flights in the FR phase. No clear bias can be seen in the OR period. The standard deviation between about 20 km and 30 km exceeds the estimated precision in the OR phase.

3.9 Additional v8 products: C₂H₂, C₂H₆, COCl₂, OCS, and CH₃Cl

Some more target molecules have been operationally processed by the v8 algorithm. To date,
425 an intercomparison study is only available **for COCl₂** (Pettinari et al., 2021). Similar to the additional v7 gases, the emissions of spectral lines of the v8 molecules are also weak compared to the spectral signatures of the standard gases (before v7). Hence, retrievals of these additional species are challenging.

C₂H₂ is mainly produced by biomass burning and, to a lesser extent, by biofuel burning (e.g. Singh et al., 1996; Parker et al., 2011; Wiegele et al., 2012). Differences are within ± 50 % up to 24 km (see Fig. 18). A significant negative bias (within -50 % difference limit) is evident in the FR mode (except for 15-16 km). A significant negative bias below 20 km and above 23 km can be seen in the OR mode (exceeding combined systematic errors and the -50 % difference limit). Lower stratospheric altitude regions in MIPAS-E retrievals sometimes show negative VMRs (in Arctic winter). Hence, this species should be carefully used in scientific studies.

C₂H₆ is produced by biomass burning, natural gas losses and fossil fuel production (e.g. Rudolph, 1995; Xiao et al., 2008; Glatthor et al., 2009). Differences are within ± 25 % up to 19 km (see Fig. 19). While a significant negative bias in MIPAS-E is obvious in the FR period (exceeding the -50 % limit above 13 km), no bias is seen in the MIPAS-E data below 20 km in the OR mode, where differences are within a ± 20 % range. Lower stratospheric altitude regions in MIPAS-E retrievals sometimes show negative VMRs (in the Arctic).

COCl₂ is produced by chemical industries and OH-initiated oxidation of chlorinated hydrocarbons in the troposphere (Kindler et al., 1995; Fu et al., 2007; Valeri et al., 2016). Figure 20 shows that differences are within ± 20 % up to 27 km in both observation periods, such that the general profile shapes (as measured by MIPAS-B) are reproduced by the satellite instrument. A negative bias is evident in the FR and OR period (except for 22-27 km), unexplained at high altitudes. Deviations in the Tropics are quite large. The deviations are in line with the findings of Pettinari et al. (2021) who compared v8 data not only to MIPAS-B but also to observations from ACE-FTS. Pettinari et al. (2021) found that some of the differences between MIPAS-E and MIPAS-B can be attributed to the different spectroscopic data used (Toon et al. (2001) for MIPAS-B and Tchana et al. (2015) in the case of MIPAS-E).

OCS is the most prevalent sulphur-containing species which is transported into the stratosphere where it acts as a precursor for the stratospheric aerosol layer (Crutzen, 1976; Kremser et al., 2016; Glatthor et al., 2017). Differences are within ± 20 % up to 24 km in the FR period and within ± 25 % up to 25 km in the OR period (see Fig. 21). A significant positive bias is visible below 22 km and a negative bias above this altitude in the OR period exceeding the ± 50 % limit and the combined systematic errors above 24 km. The agreement between the VMR profiles of both sensors is better in the FR period. Here, a significant (positive) bias is only visible between 14 and 18 km. Deviations in the Tropics are quite large.

460 CH₃Cl is the most abundant halocarbon in the atmosphere and originates from natural and anthropogenic sources (see e.g. Yokouchi et al., 2000). Fig. 22 shows that differences stay within $\pm 20\%$ between 13 and 22 km (full observation period). However, the comparison reveals a positive bias above 16 km and a negative bias below this altitude in the FR period. A negative bias within -35% between 19 and 26 km, increasing with altitude, and exceeding the combined
465 systematic errors above 26 km is also visible in the OR period. Large deviations between both instruments occur at midlatitudes and in the Tropics.

4 Conclusions

Vertical profiles of MIPAS balloon flights between 2002 and 2011 covering virtually the whole
470 lifetime of MIPAS on ENVISAT have been used for an intercomparison study of all operational parameters delivered by ESA (except HDO), namely temperature and 20 species as listed in Table 1. The main findings of this intercomparison study are summarized in Table 4. The difference between retrieved temperature profiles of both MIPAS instruments generally stays within ± 2 K in the stratosphere. The MIPAS satellite observations of a large number of gases
475 like H₂O, O₃, HNO₃, CH₄, N₂O, NO₂, N₂O₅, ClONO₂, CFC-11, CFC-12, HCFC-22, CCl₄, CF₄, COF₂, and HCN show an overall good agreement of 5 % to 20 % with the MIPAS balloon measurements in the lower stratosphere.

The intercomparison of the new MIPAS-E v8 products C₂H₂, C₂H₆, COCl₂, OCS, and CH₃Cl exhibits a somewhat poorer agreement with the MIPAS-B observations compared to the above-
480 mentioned species. However, COCl₂, OCS, and CH₃Cl achieve a 20-percent agreement at least in the extratropical upper troposphere and lower stratosphere.

Overall it can be stated that the v8 operational MIPAS-E data can be recommended for scientific use. However, data users are strongly advised to consider the findings presented in this study in the respective sections and in Table 4 when using the MIPAS-E data. A comprehensive
485 MIPAS-E quality readme file not only including the validation results related to MIPAS-B, but in addition ground-based and ACE-FTS validation results was published by Raspollini et al. (2020) and is recommended for data users who want to get more detailed information on the quality of the MIPAS satellite data.

490 *Data availability.* MIPAS operational satellite data are available at the European Space Agency mission web page (<https://doi.org/10.5270/EN1-c8hgqx4>, last access: 12 July 2022). MIPAS balloon data are available upon request (<https://www.imk-asf.kit.edu/ffb.php>, last access: 12 July 2022).

495 *Author contributions.* GW wrote the paper and performed the bulk of the MIPAS balloon data analysis, with input from all co-authors. AK performed the MIPAS-B Level 1 data processing. MH provided the retrieval software. FFV and GM operated the balloon instrument during all campaigns. HO directed the research and flight planning. MS used a 1-dimensional model for photochemical corrections. JA performed trajectory match calculations. PR had a leading role
500 in evaluating and improving the MIPAS ESA data. AD was the head of the MIPAS Quality Working Group and coordinated the validation activities. All authors commented on and improved the manuscript.

Competing interests. The authors declare that they have no conflict of interest.

505

Special issue statement. This article is part of the special issue “MIPAS ESA Level 2 version 8 products: algorithms, product features and validation”. It is not associated with a conference.

Acknowledgements. Financial support by the DLR (Project 50EE0020) and ESA for the MIPAS
510 balloon flights is gratefully acknowledged. We thank the Centre National d'Etudes Spatiales (CNES) balloon launching team and the Swedish Space Corporation (SSC) Esrange team for excellent balloon operations. An acknowledgement goes to the work performed by the Quality Working Group established by ESA for verification and monitoring of MIPAS products. A corresponding report on the validation activities was published by ESA (Wetzel et al., 2020).
515 We acknowledge support by Deutsche Forschungsgemeinschaft and the Open Access Publishing Fund of Karlsruhe Institute of Technology.

Table 1. Overview of MIPAS-E spectral windows used for the analysis of atmospheric target parameters together with typical precision errors and total errors (OR mode, winter) in the altitude range of the compared MIPAS balloon measurements.

Target parameter	Spectral range (cm ⁻¹)	Precision error	Total error
Temperature	703.4 – 792.3 937.5 – 944.6	0.1 – 0.2 K	0.8 – 2.5 K
H ₂ O	953.6 – 956.6 1224.8 – 1227.8 1402.6 – 1577.1	0.1 – 3 %	8 – 28 %
O ₃	729.3 – 759.6 1043.9 – 1046.9 1117.0 – 1126.6	0.1 – 2 %	7 – 13 %
HNO ₃	836.9 – 921.9	0.5 – 10 %	5 – 20 %
CH ₄	1219.1 – 1307.6	0.1 – 2 %	10 – 20 %
N ₂ O	1230.4 – 1279.3	0.1 – 3 %	8 – 18 %
NO ₂	1570.5 – 1629.0	0.3 – 4 %	11 – 30 %
N ₂ O ₅	1220.0 – 1247.6	0.5 – 20 %	13 – 50 %
ClONO ₂	777.4 – 810.4 1724.0 – 1746.2	0.3 – 10 %	3 – 25 %
CFC-11	842.9 – 852.5	0.2 – 20 %	5 – 25 %
CFC-12	857.5 – 940.1	0.2 – 20 %	5 – 25 %
HCFC-22	803.4 – 839.6	0.2 – 18 %	6 – 25 %
CCl ₄	792.8 – 795.8	0.5 – 15 %	12 – 30 %
CF ₄	1256.7 – 1286.3	0.2 – 4 %	14 – 30 %
COF ₂	772.0 – 775.0 1222.4 – 1235.8	1 – 10 %	8 – 30 %
HCN	711.1 – 762.4 1370.0 – 1372.1	1 – 20 %	6 – 60 %
C ₂ H ₂	763.3 – 772.9	17 – 68 %	20 – 70 %
C ₂ H ₆	819.2 – 845.4	16 – 72 %	23 – 85 %
COCl ₂	839.3 – 862.8	6 – 60 %	22 – 62 %
OCS	840.6 – 857.0 2050.2 – 2053.2	6 – 89 %	9 – 90 %
CH ₃ Cl	738.2 – 752.7 1458.4 – 1461.4	8 – 50 %	32 – 90 %

Table 2. Overview of MIPAS-B spectral windows used for the analysis of atmospheric target parameters together with typical precision errors and total errors.

Target parameter	Spectral range (cm ⁻¹)	Precision error	Total error
Temperature	801.1 – 813.2 941.3 – 956.7	0.2 – 0.3 K	0.5 – 1.0 K
H₂O	808.0 – 825.3 1210.2 – 1244.5 1585.0 – 1615.0	1 – 2 %	8 – 11 %
O₃	763.5 – 824.4 964.9 – 969.0 1140.1 – 1195.6	0.1 – 1 %	8 – 10 %
HNO₃	864.0 – 874.0	0.2 – 2 %	8 – 9 %
CH₄ & N₂O	1161.9 – 1229.8	1 – 3 %	6 – 10 %
NO₂	1585.0 – 1615.0	1 – 3 %	10 – 12 %
N₂O₅	1220.0 – 1270.0	0.4 – 2 %	5 – 7 %
ClONO₂	779.7 – 780.7	2 – 3 %	5 – 6 %
CFC-11	840.0 – 860.0	2 – 3 %	5 – 6 %
CFC-12	918.0 – 924.0	2 – 3 %	5 – 6 %
HCFC-22	828.0 – 830.0	3 – 6 %	9 – 12 %
CCl₄	786.0 – 806.0	5 – 10 %	11 – 15 %
CF₄	1274.3 – 1288.0	2 – 6 %	6 – 11 %
COF₂	750.0 – 776.0	1 – 3 %	10 – 12 %
HCN	750.0 – 776.0	4 – 8 %	9 – 12 %
C₂H₂	750.2 – 790.1	5 – 10 %	7 – 12 %
C₂H₆	811.5 – 835.8	8 – 12 %	12 – 15 %
COCl₂	838.3 – 860.0	2 – 5 %	20 – 22 %
OCS	842.4 – 876.0	15 – 20 %	18 – 25 %
CH₃Cl	742.5 – 755.0	5 – 15 %	12 – 20 %

535 **Table 3.** Overview of MIPAS balloon flights used for intercomparison with MIPAS-E. Distances and times between closest trace gas profile pairs observed by MIPAS-E and the validation instrument refer to an altitude of 20 km (Kiruna) and 30 km (Aire sur l'Adour and Teresina). In addition, 2-day forward/backward trajectories were calculated for each balloon flight to search for further matches with the satellite sensor.

Location	Date	Distance (km)	Time difference (min)
Kiruna, 68 °N	20 Mar 2003	16 / 546	14 / 15
	03 Jul 2003	Trajectories only	
	11 Mar 2009	187 / 248	5 / 6
	24 Jan 2010	109 / 302	5 / 6
	31 Mar 2011	Trajectories only	
Aire sur l'Adour, 44 °N	24 Sep 2002	21 / 588 / 410 / 146	12 / 13 / 15 / 16
Teresina, 5 °S	14 Jun 2005	109 / 497 / 184 / 338	228 / 229 / 268 / 269
	06 Jun 2008	224 / 284 / 600 / 194	157 / 158 / 169 / 170

540

545

550

Table 4. Summary of MIPAS-E validation results (trajectory comparison to eight MIPAS-B flights). Mentioned atmospheric parameter differences refer to MIPAS-E minus the balloon instrument.

Parameter	Comments (L1v8/L2v8 FM)
Temp.	Differences within ± 2 K between 12 and 39 km.
H₂O	Positive bias (5-20 %) between 11 and 39 km within combined systematic errors (except OR mode around 15 km).
O₃	Differences within ± 10 % for all altitudes above 15 km.
HNO₃	Significant positive bias (5-20 %) below 27 km (most pronounced between 19 and 26 km in the OR mode).
CH₄ & N₂O	Positive bias for CH ₄ (5-15 %) and N ₂ O (10-20 %) below 35 km (within combined systematic errors), especially pronounced for N ₂ O in the lowermost stratosphere around 15 km. Somewhat larger positive deviations also in the Tropics around 30 km.
NO₂	Positive bias of up to 20 % in FR mode (unexplained above 31 km), smaller positive bias (~ 10 %) in OR mode (above 27 km).
N₂O_s	Differences within ± 10 % between 24 and 34 km (no significant bias in OR mode, small negative bias in FR period).
ClONO₂	Differences within ± 10 % between 17 and 34 km (no significant bias).
CFC-11	Differences within 10 % below 20 km. Positive bias (increasing with altitude) above this altitude level.
CFC-12	Differences within ± 5 % for altitudes below 20 km. Significant positive bias above this altitude level up to 32 km.
HCFC-22	Differences within ± 10 % up to 26 km (FR mode) and 28 km (OR mode). Positive differences up to 20 % above 26 km (FR mode) and significant negative bias above 28 km (OR mode).
CCl₄	Differences within ± 20 % up to about 22 km in both observation periods. Increasing negative bias above 22 km (full period).
CF₄	Differences within ± 10 % between 11 and 37 km (both periods). Significant positive bias above 10 km in FR period. No clear bias in OR period.
COF₂	Differences within ± 10 % for FR period and within ± 20 % in OR period in the stratosphere; no unexplained biases.
HCN	Differences within ± 20 % below 34 km. Stratospheric positive bias in FR mode, exceeding combined systematic errors above 20 km (difference > 20 %). No clear bias in OR period.
C₂H₂	Differences within ± 50 % up to 24 km. Negative bias (within 50 %) in FR mode (except 15-16 km), significant negative bias below 20 km and above 23 km in OR mode (exceeding combined systematic errors and the -50 % difference limit). Lower stratospheric altitude regions in MIPAS-E retrievals sometimes show negative VMRs (in Arctic winter).
C₂H₆	Differences within ± 25 % up to 19 km. Significant negative bias in FR mode (exceeding -50 % limit above 13 km), no bias in OR mode below 20 km (differences within ± 20 %). Lower stratospheric altitude regions in MIPAS-E retrievals sometimes show negative VMRs (in the Arctic).
COCl₂	Differences within ± 20 % up to 27 km in both periods. Negative bias in FR and OR period (except 22-27 km), unexplained at high altitudes; quite large deviations in the Tropics. Parts of differences can be attributed to new spectroscopic data (MIPAS-E retrieval).
OCS	Differences within ± 20 % up to 24 km in FR period. Significant positive bias between 14 and 18 km; difference within ~ 25 % up to 25 km (OR mode). Significant positive bias < 22 km and negative bias > 22 km (OR mode) exceeding ± 50 % limit and combined systematic errors above 24 km; quite large deviations in the Tropics.
CH₃Cl	Differences within ± 20 % between 13 and 22 km. Positive bias above 16 km (negative bias below) in FR period. Negative bias within -35 % between 19 and 26 km, increasing with altitude, and exceeding the combined systematic errors above 26 km (OR period). Large deviations at midlatitudes and in the Tropics.

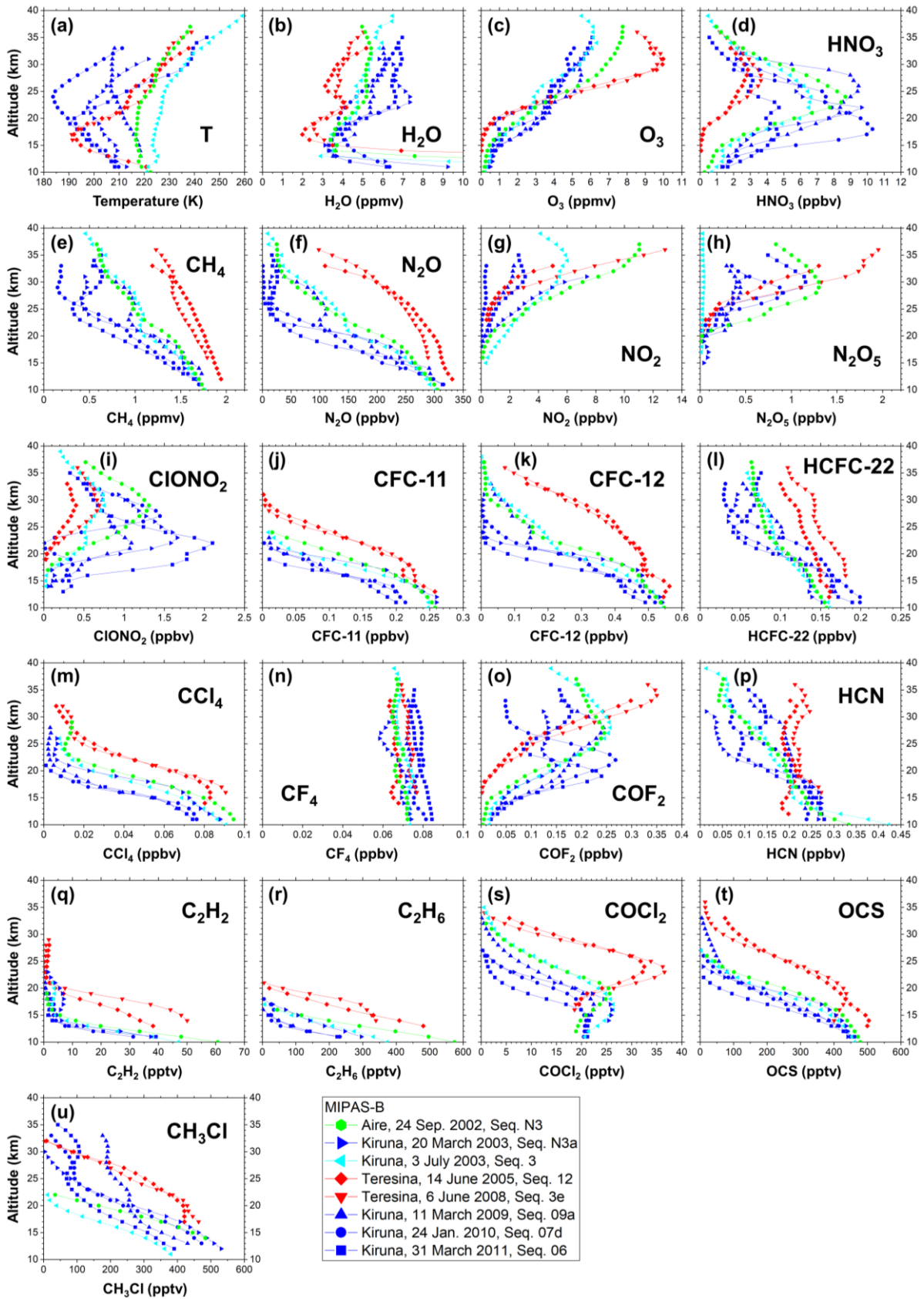


Figure 1. Retrieved vertical profiles of temperature (a) and species (b-u) of Arctic winter (blue), Arctic summer (cyan), midlatitude (green) and tropical (red) MIPAS-B flights as listed in Table 3.

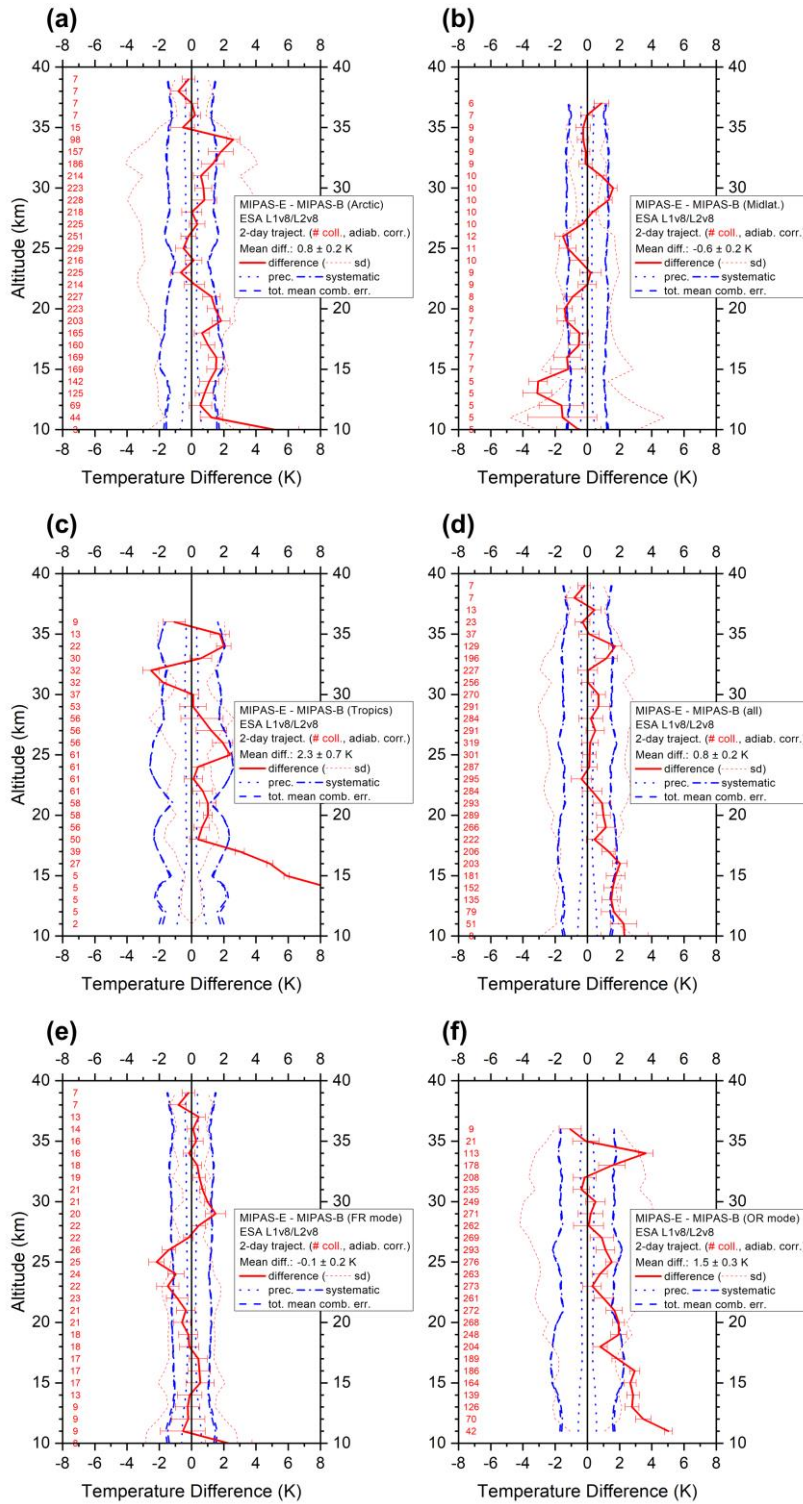


Figure 2. Mean temperature difference (red solid line) of all trajectory match collocations (red numbers) between MIPAS-E and MIPAS-B including standard deviation (red dotted lines) and standard error of the mean (plotted as error bars). Precision (blue dotted lines), systematic (blue dash-dotted lines), and total (blue dashed lines) mean combined errors are shown, too. Arctic (a), midlatitude (b), Tropics (c), all FR plus OR (d), FR mode (e), and OR mode (f) collocations. For details, see text.

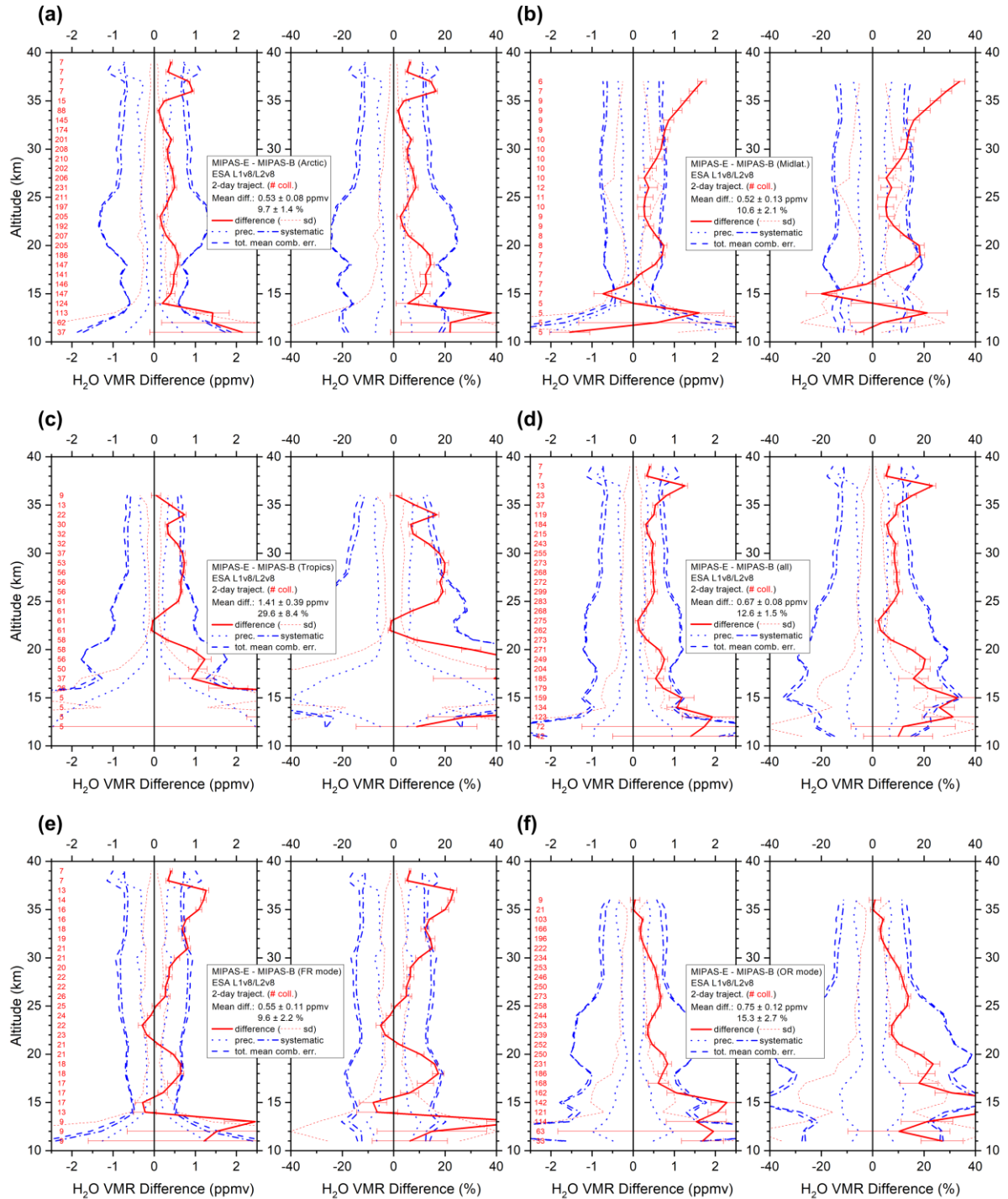


Figure 3. Mean absolute and relative H₂O VMR difference of all trajectory match collocations (red numbers) between MIPAS-E and MIPAS-B (red solid line) including standard deviation (red dotted lines) and standard error of the mean (plotted as error bars). Precision (blue dotted lines), systematic (blue dash-dotted lines), and total (blue dashed lines) mean combined errors are shown, too. Arctic (a), midlatitude (b), Tropics (c), all FR plus OR (d), FR mode (e), and OR mode (f) collocations. For details, see text.

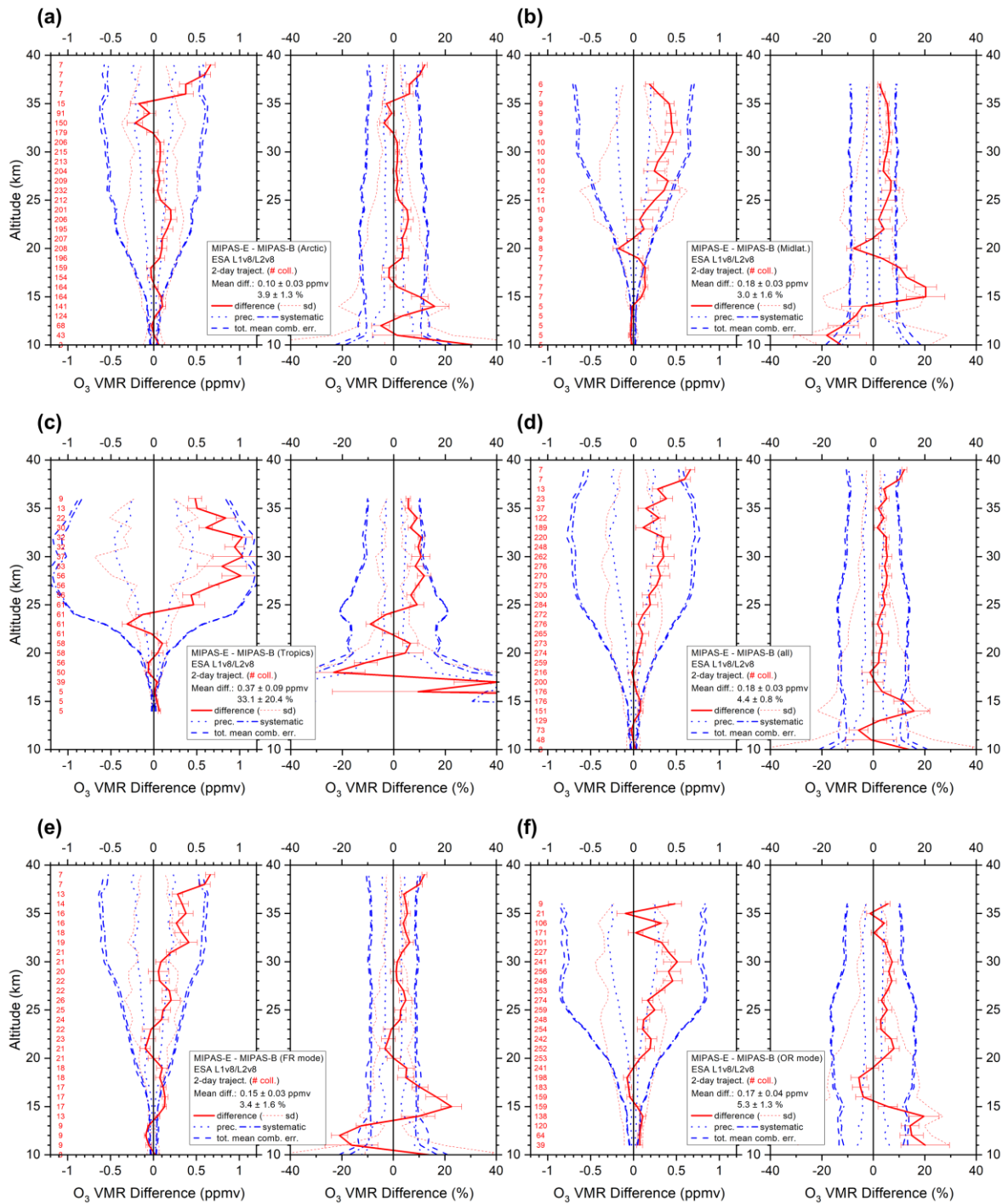


Figure 4. Same as Fig. 3 but for O₃.

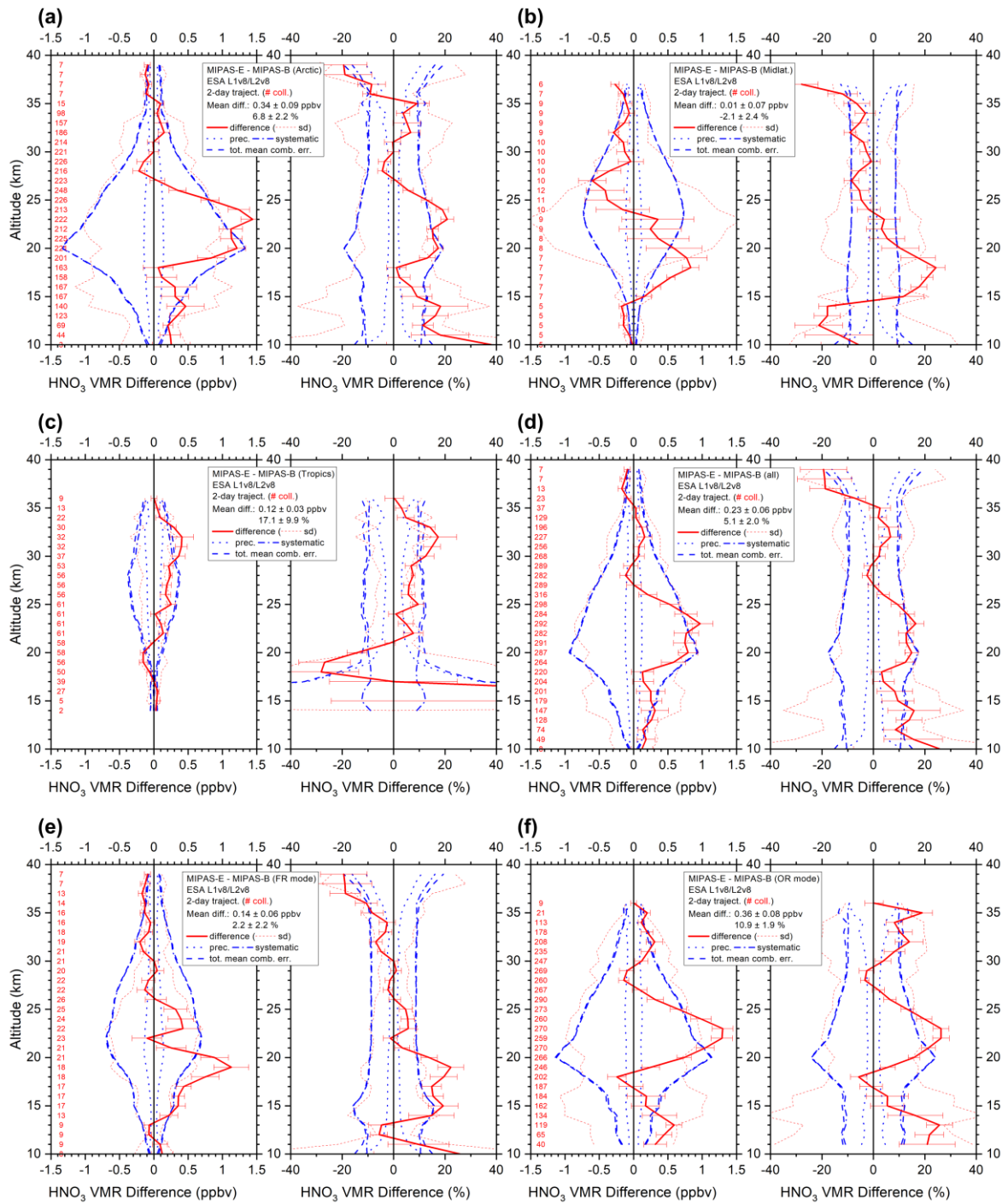


Figure 5. Same as Fig. 3 but for HNO₃.

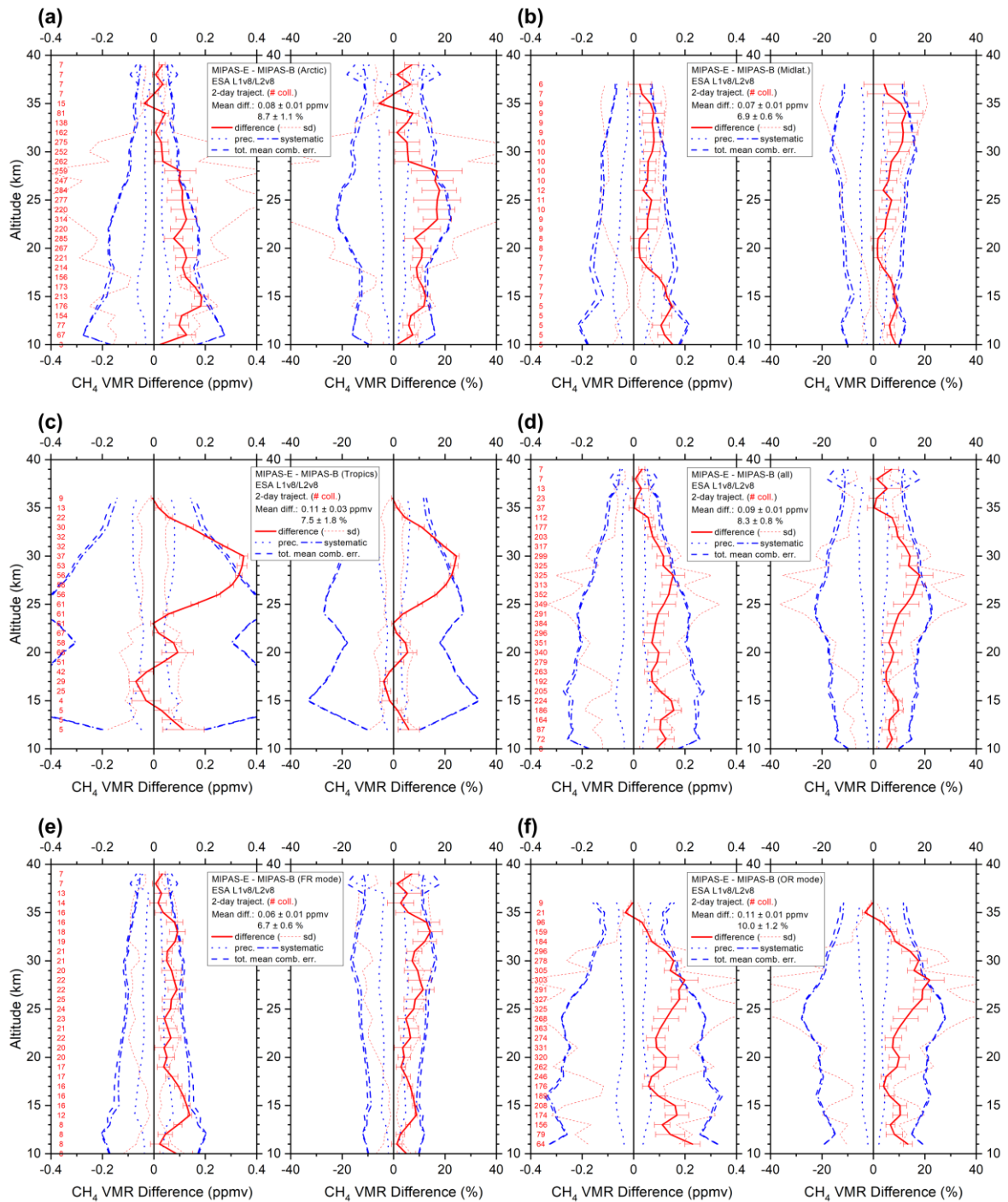


Figure 6. Same as Fig. 3 but for CH₄.

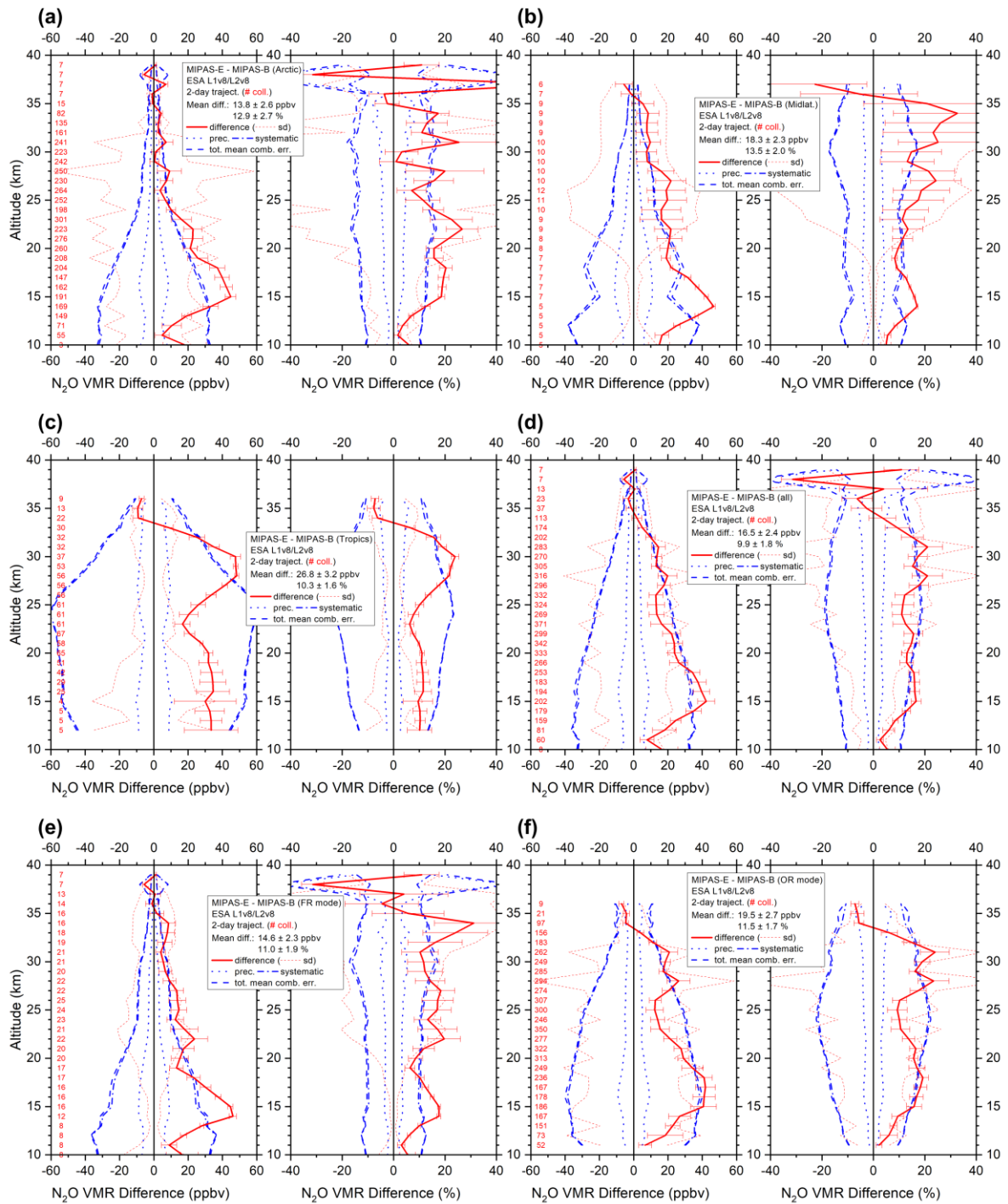


Figure 7. Same as Fig. 3 but for N₂O.

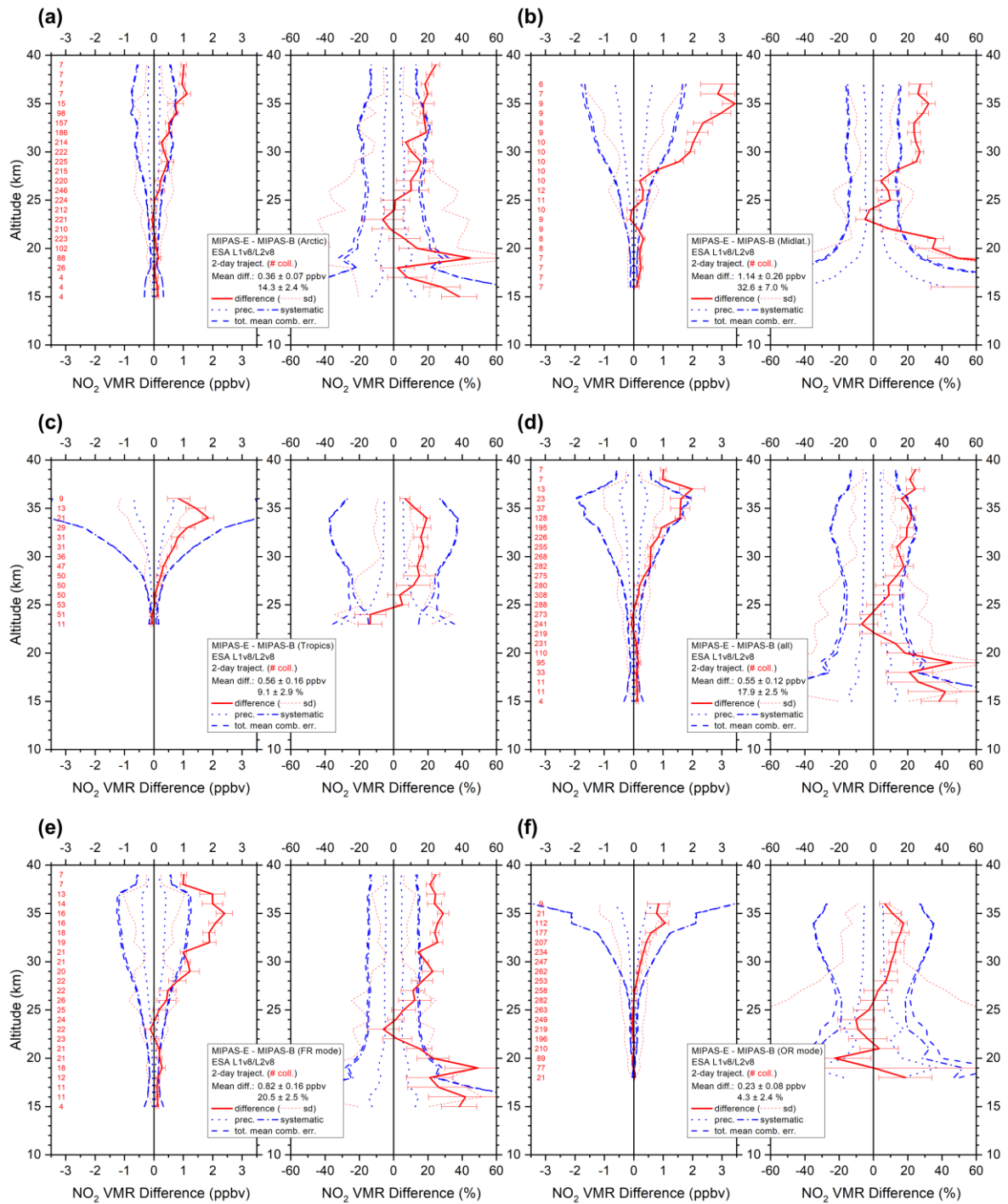


Figure 8. Same as Fig. 3 but for NO₂.

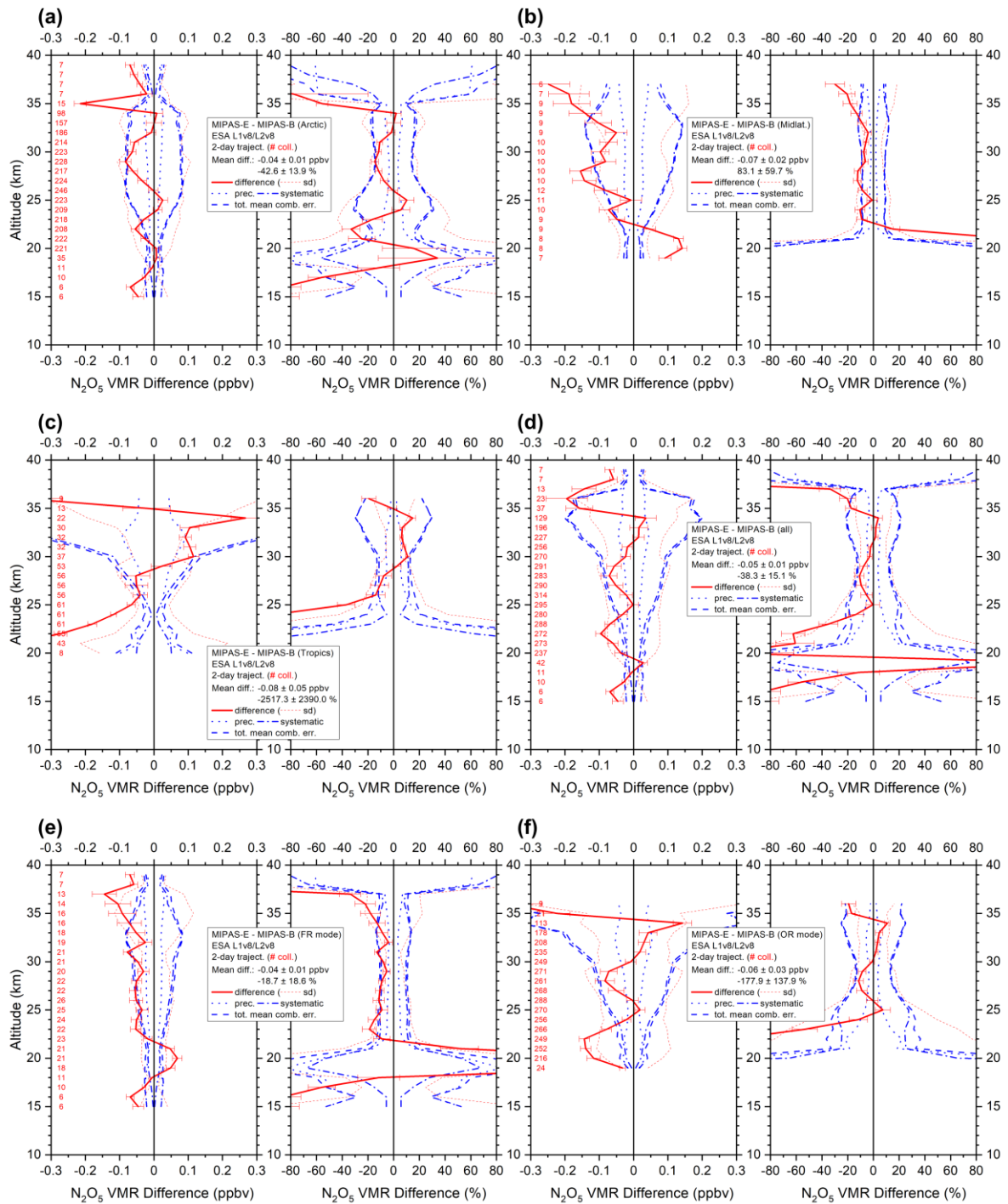


Figure 9. Same as Fig. 3 but for N_2O_5 .

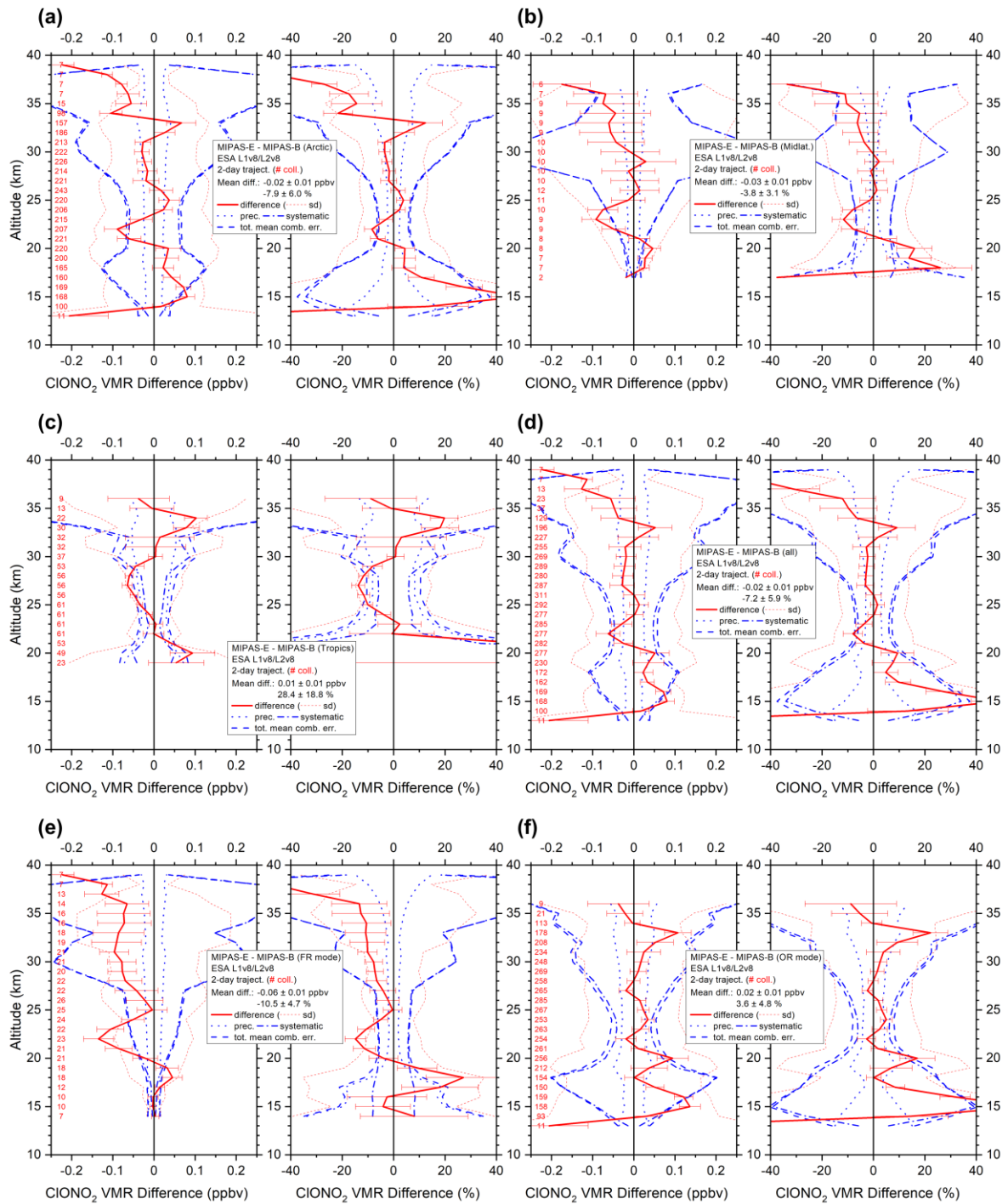


Figure 10. Same as Fig. 3 but for CIONO₂.

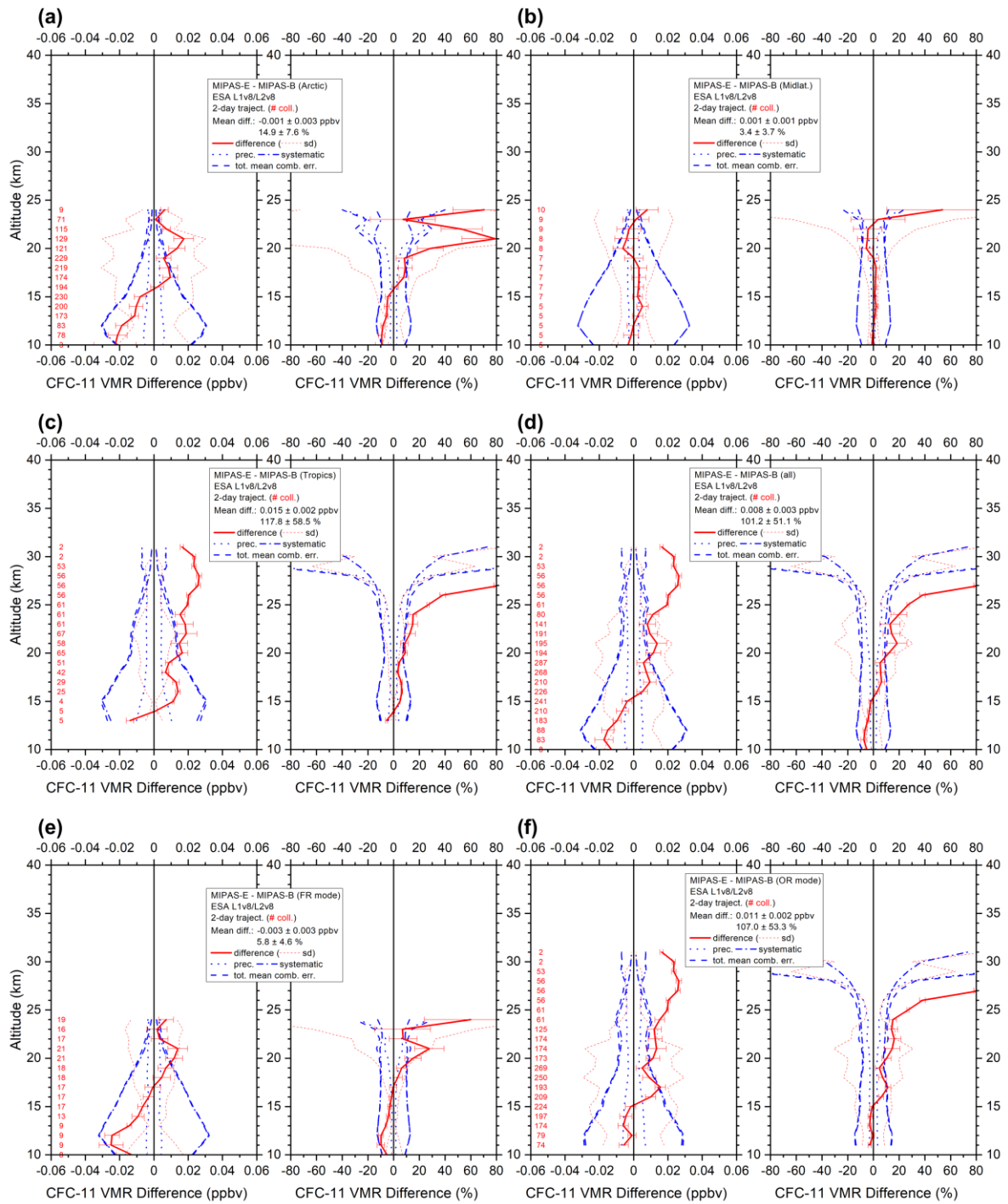


Figure 11. Same as Fig. 3 but for CFC-11.

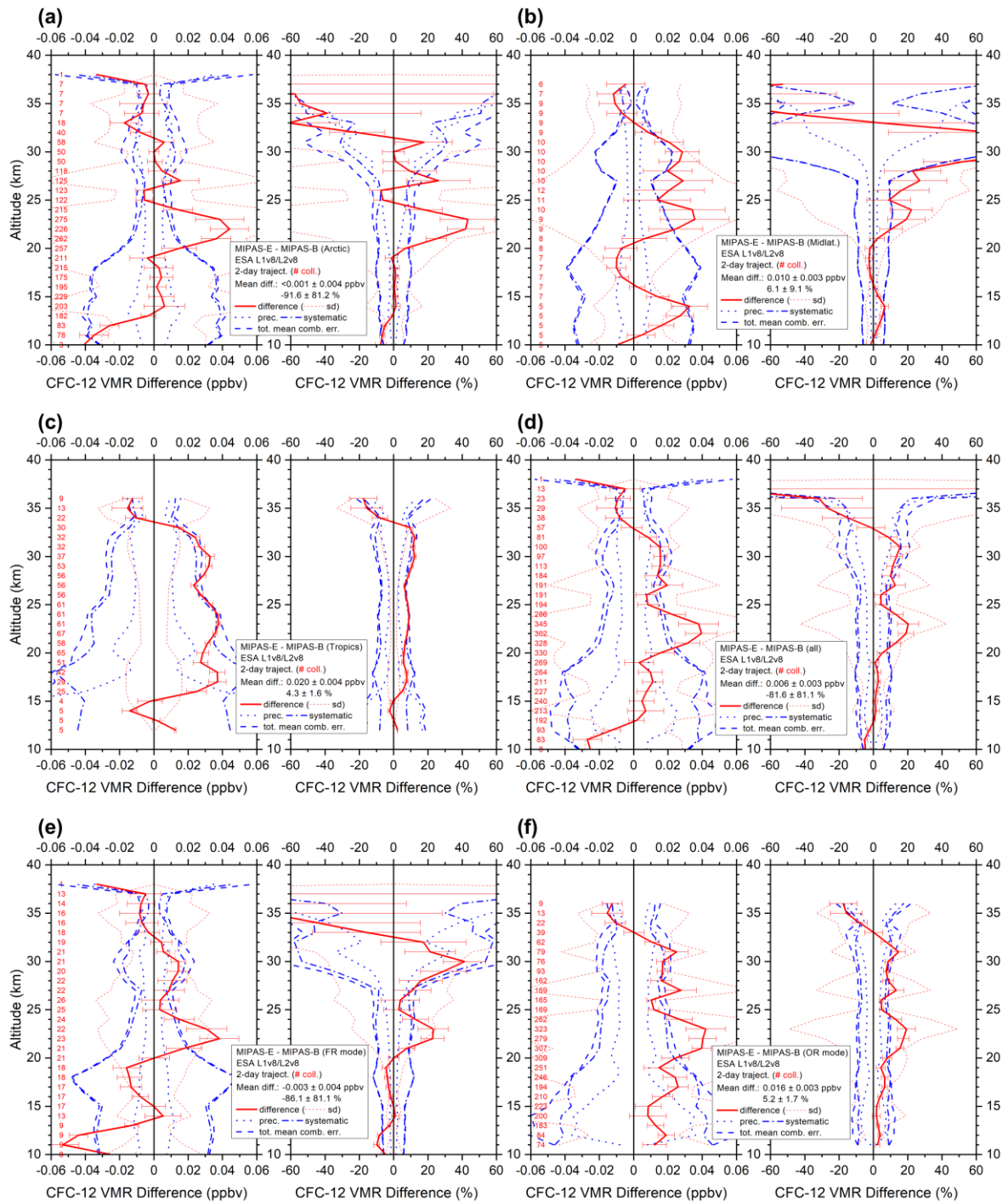


Figure 12. Same as Fig. 3 but for CFC-12.

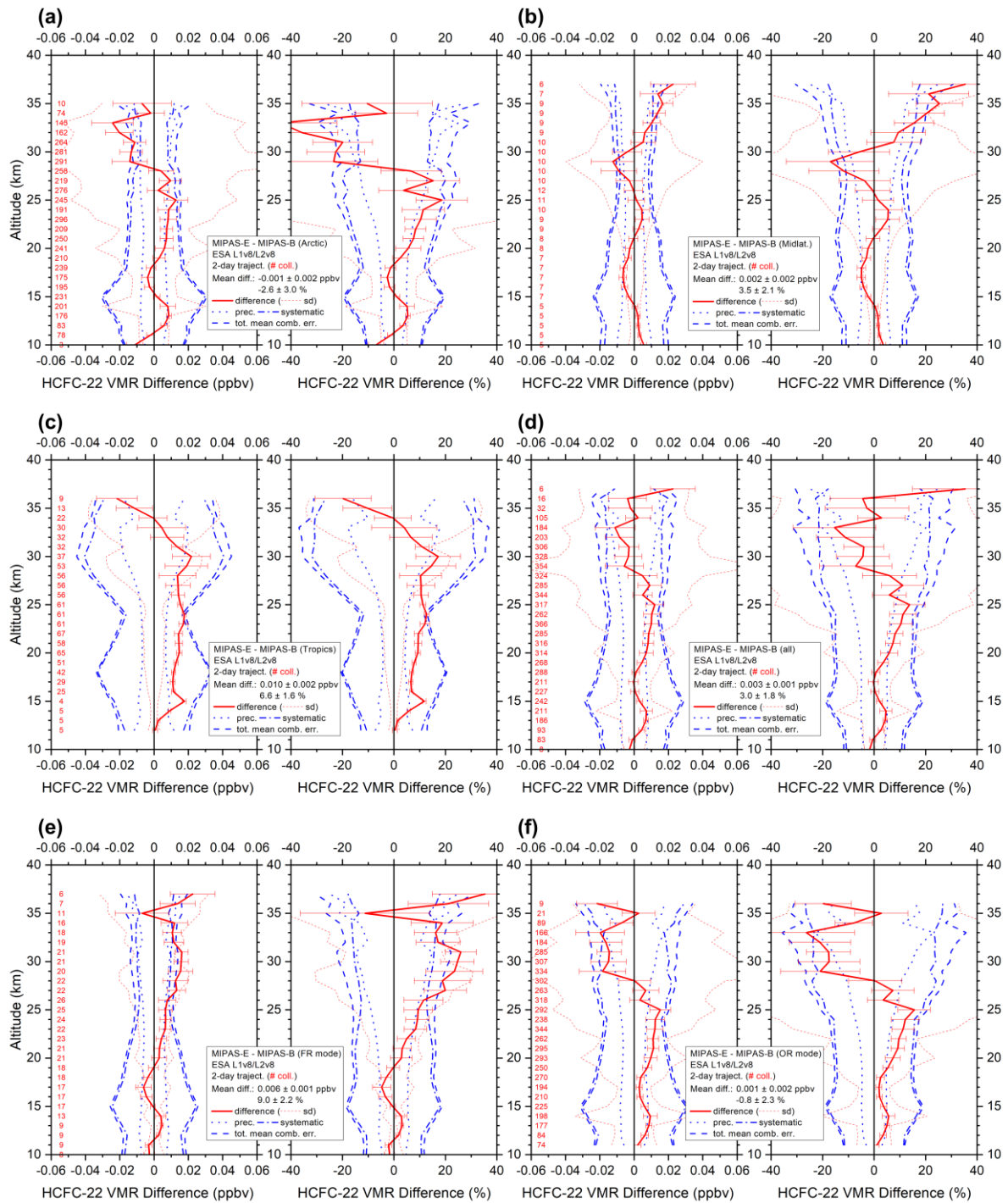


Figure 13. Same as Fig. 3 but for HCFC-22.

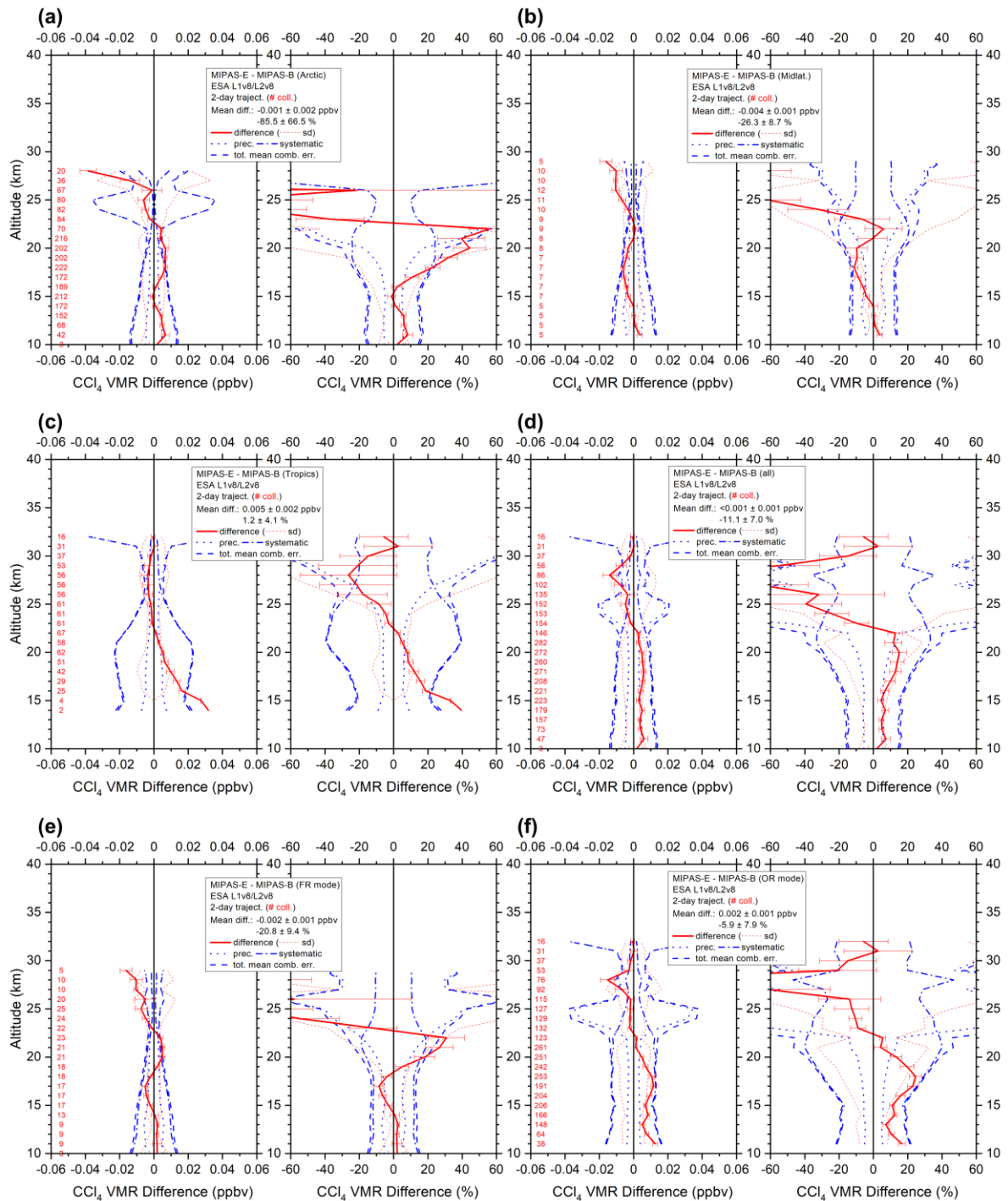


Figure 14. Same as Fig. 3 but for CCl₄.

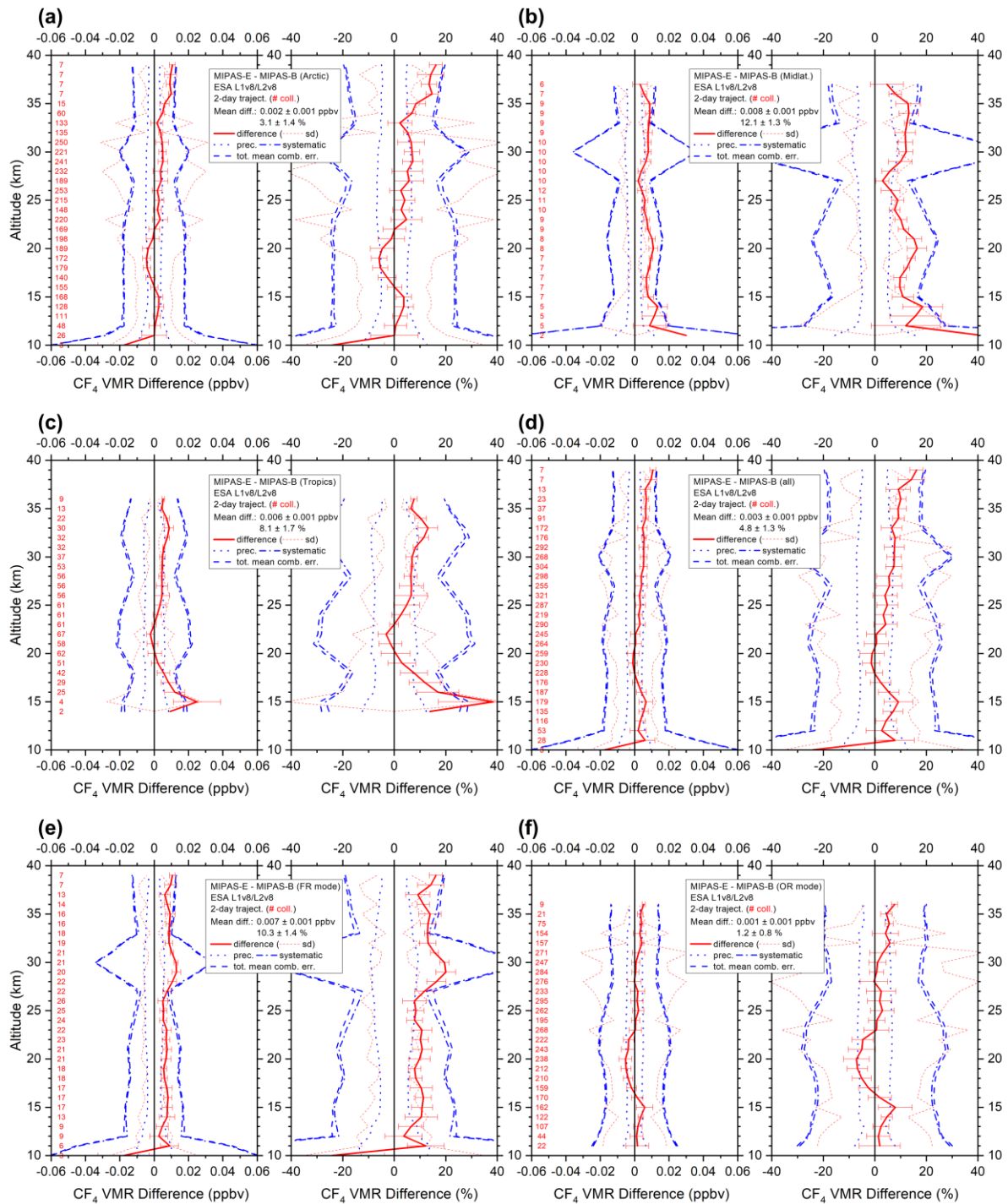


Figure 15. Same as Fig. 3 but for CF₄.

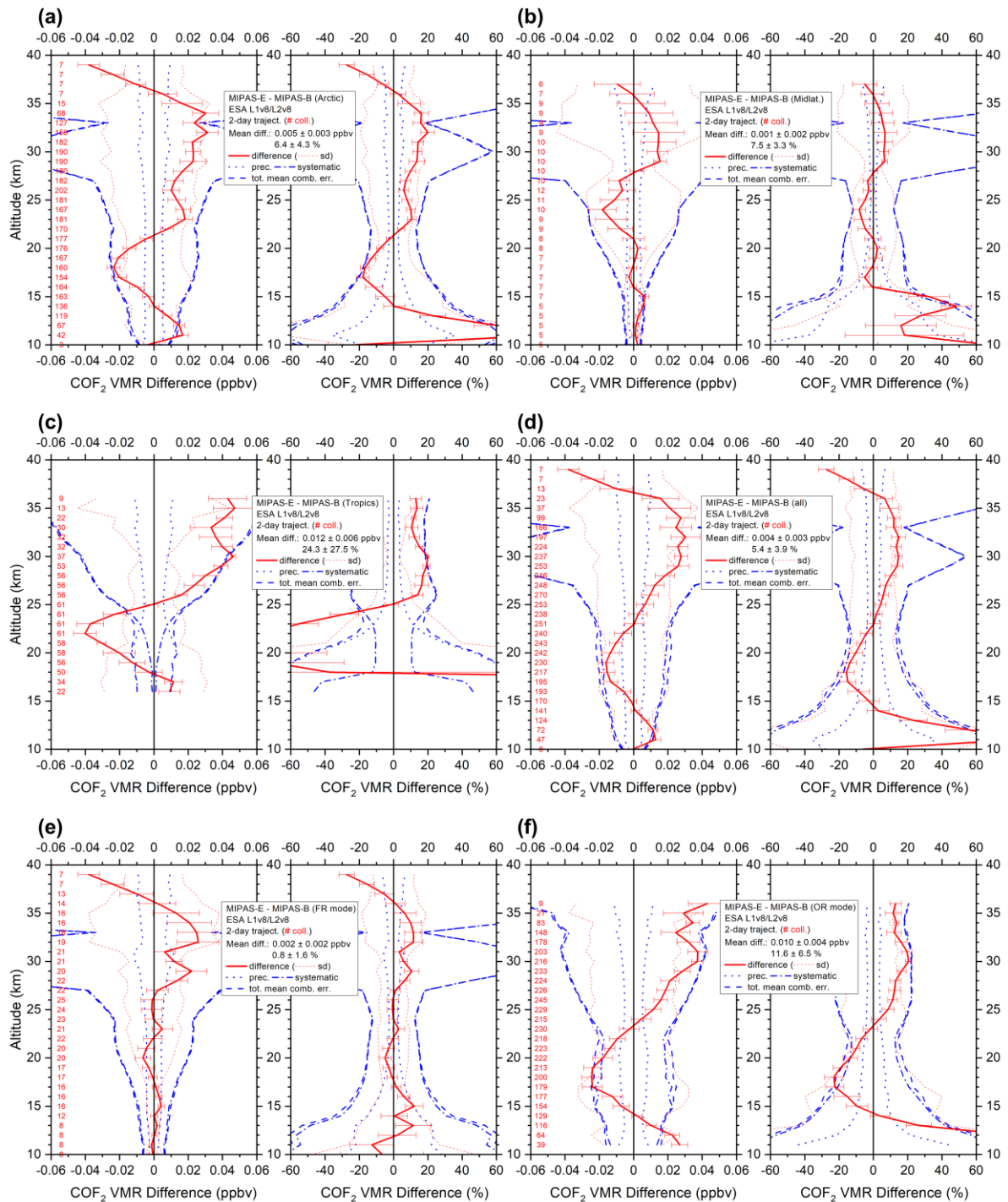


Figure 16. Same as Fig. 3 but for CO₂.

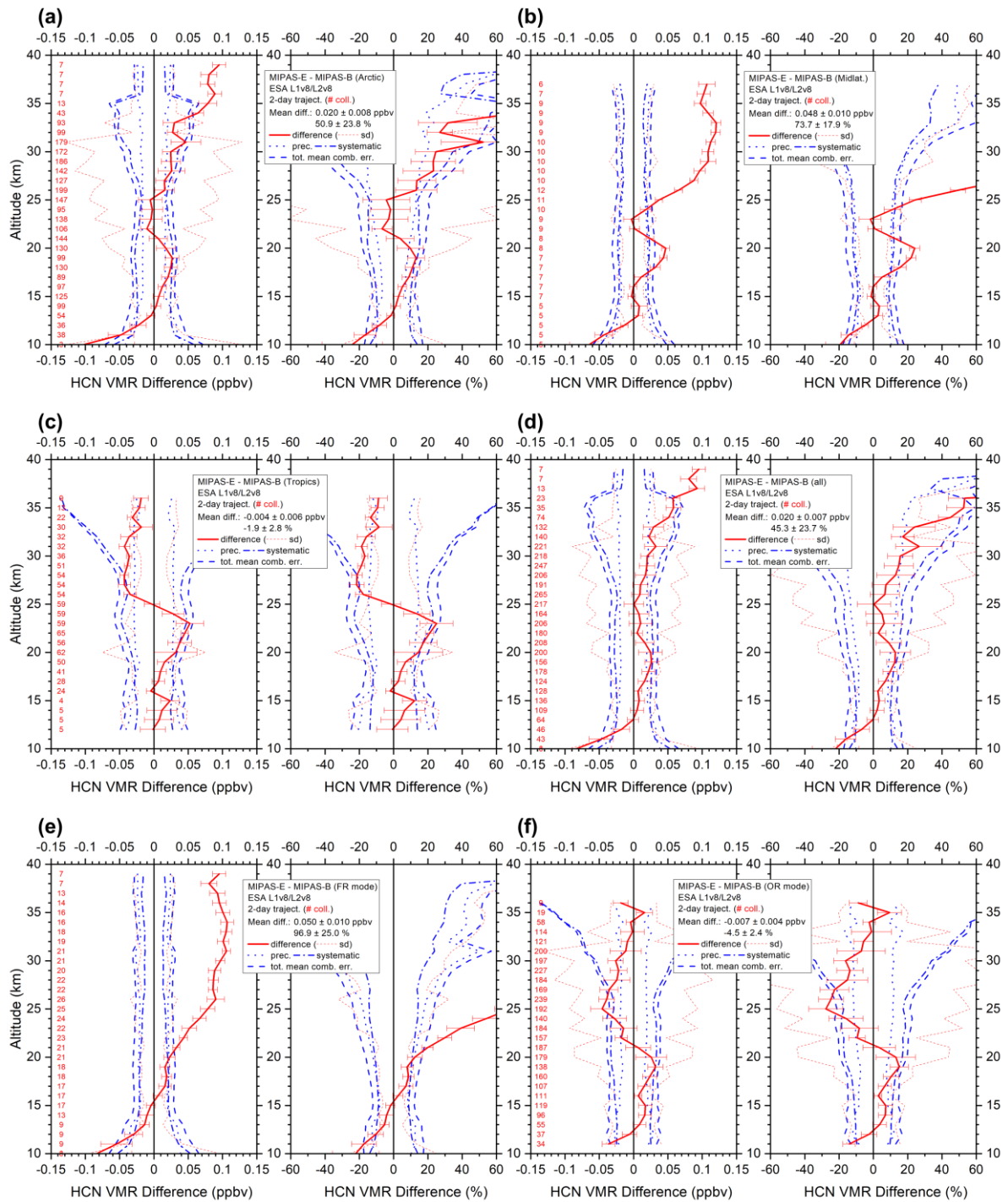


Figure 17. Same as Fig. 3 but for HCN.

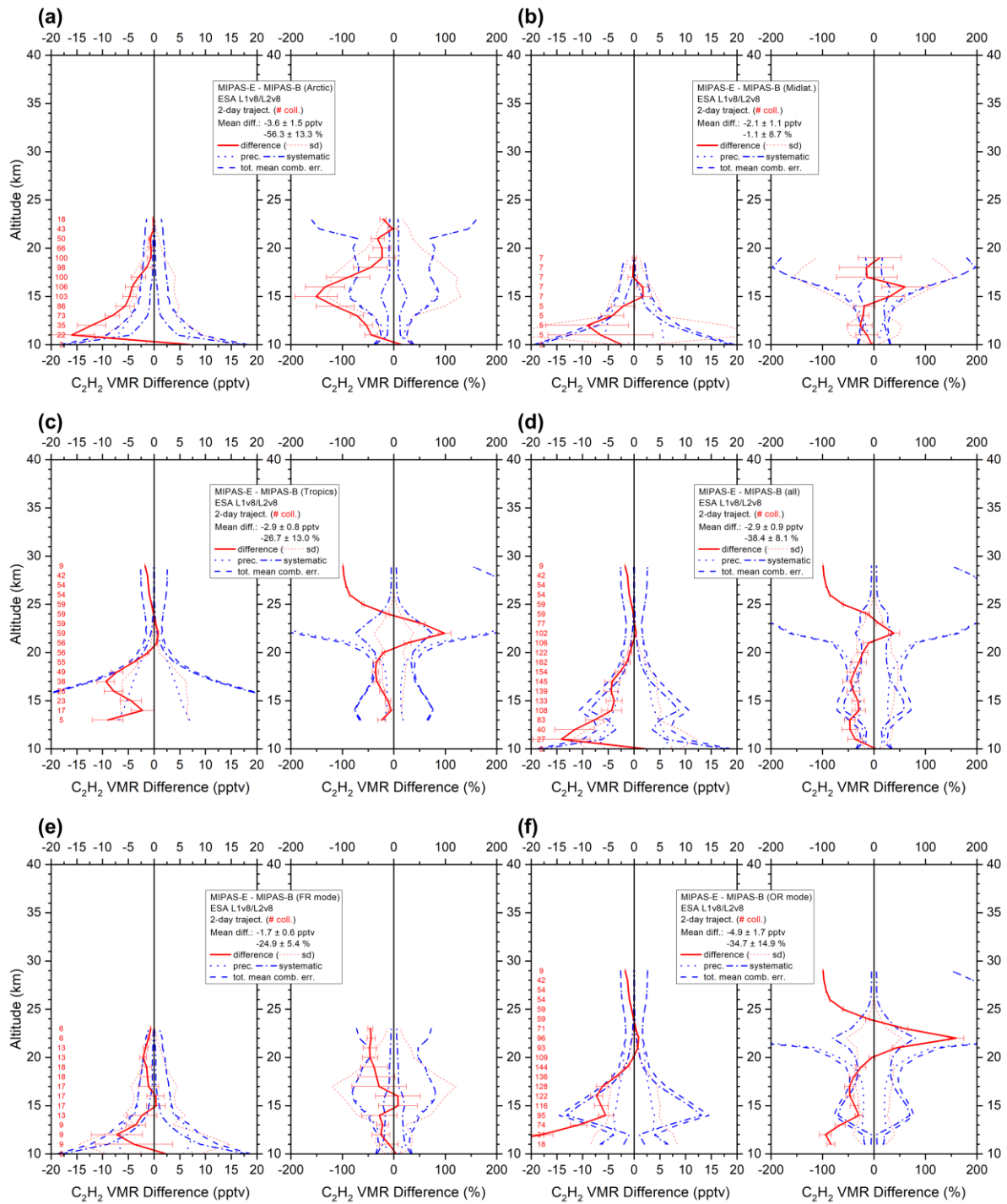


Figure 18. Same as Fig. 3 but for C_2H_2 .

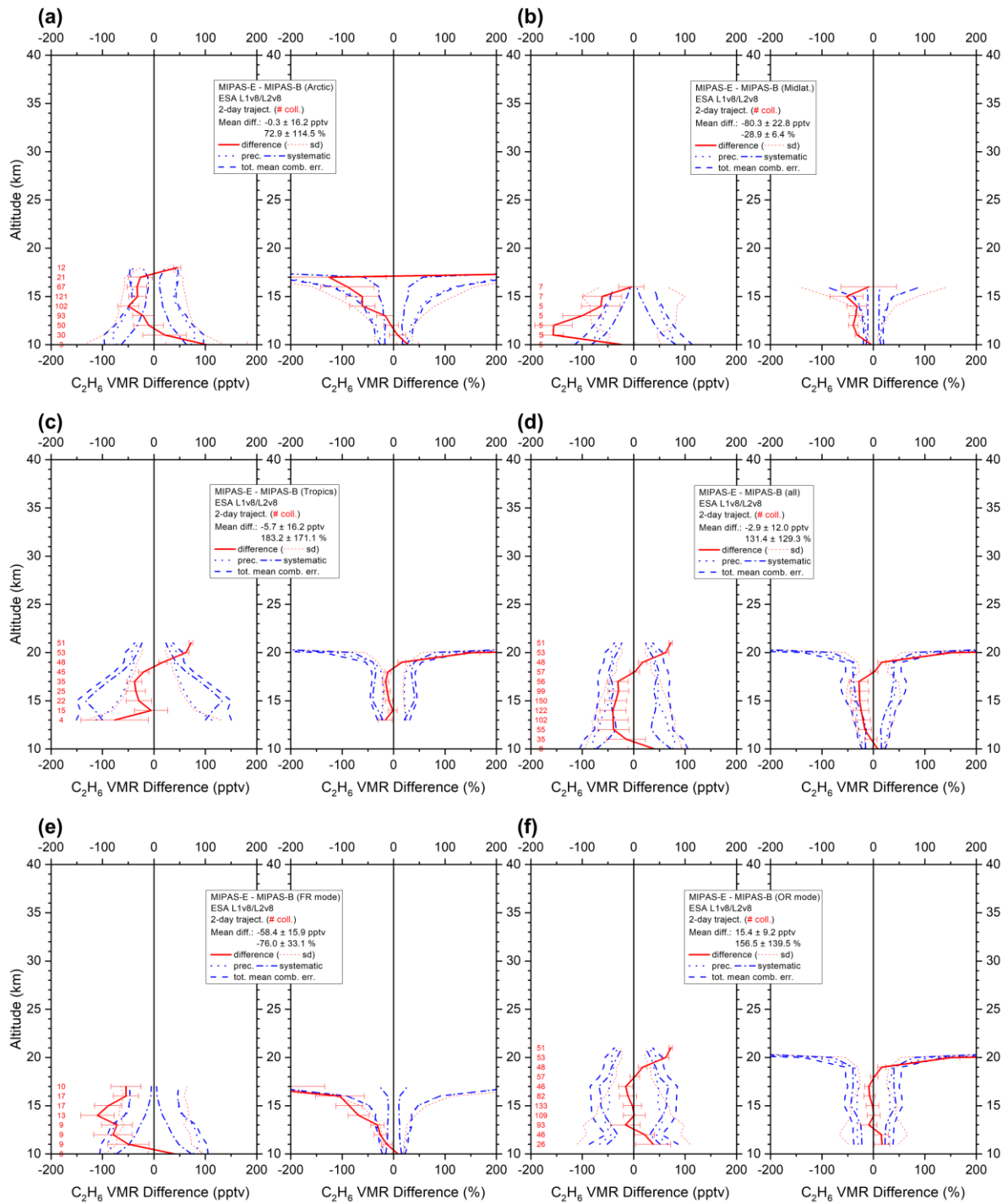


Figure 19. Same as Fig. 3 but for C_2H_6 .

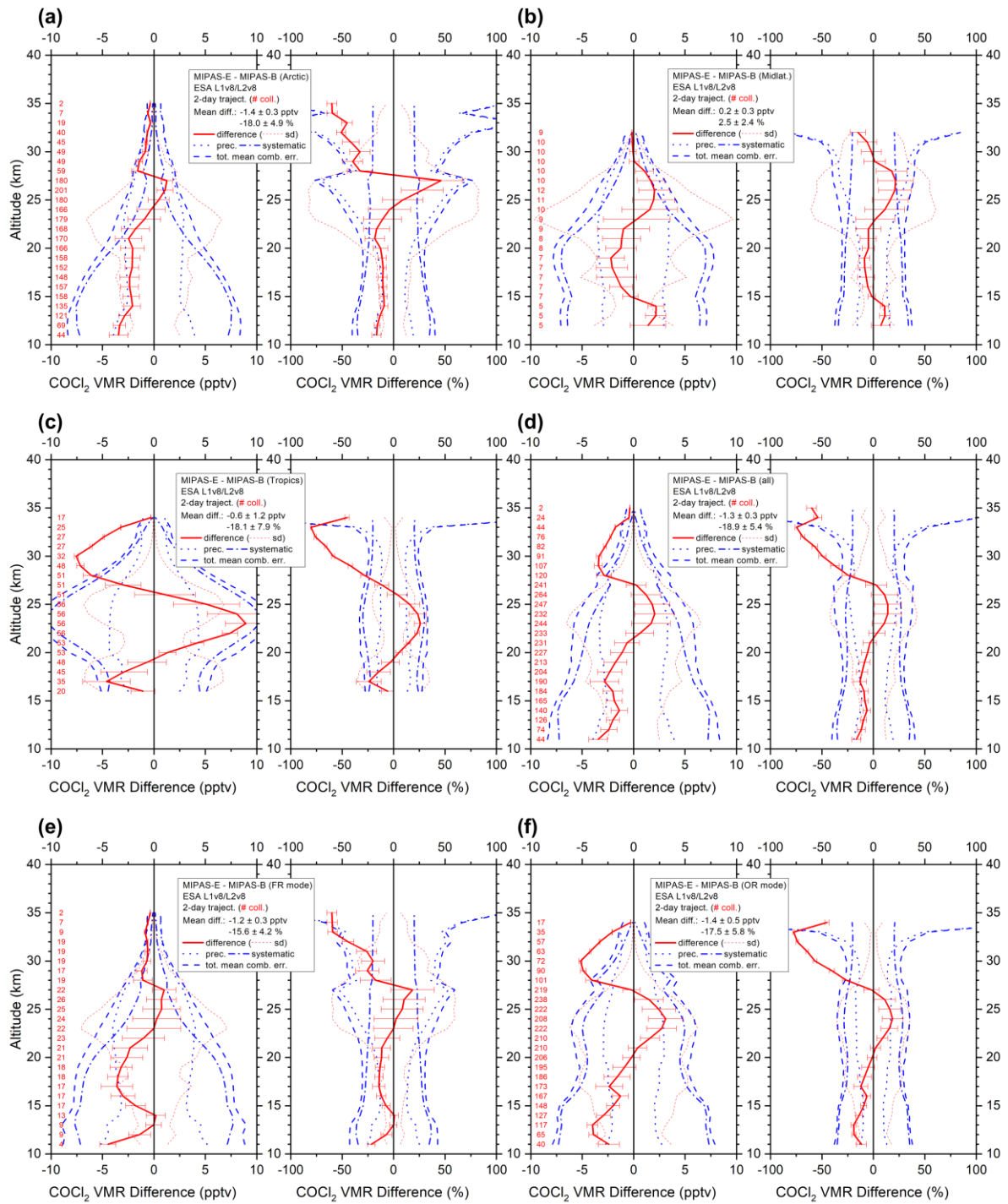


Figure 20. Same as Fig. 3 but for COCl₂.

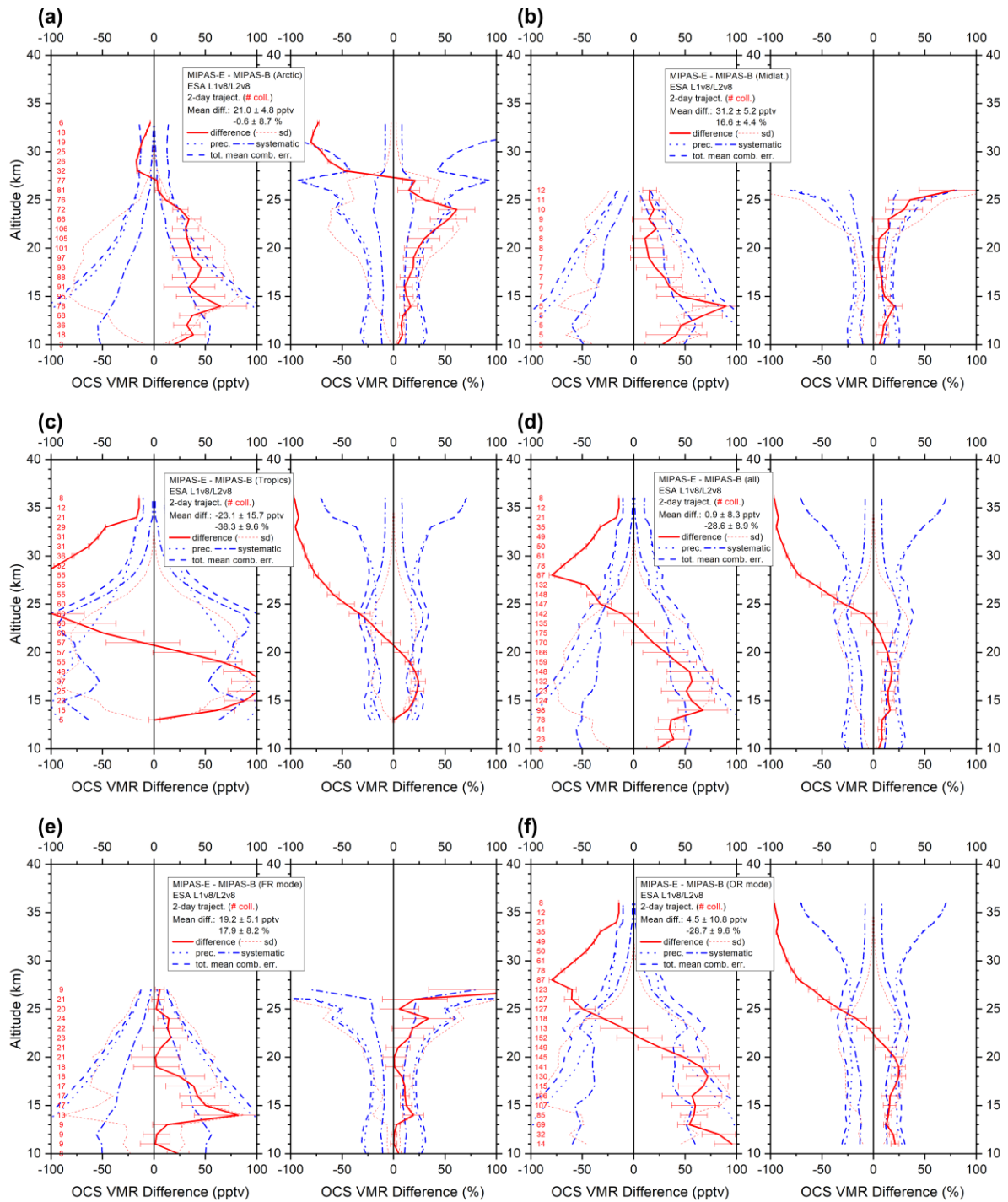


Figure 21. Same as Fig. 3 but for OCS.

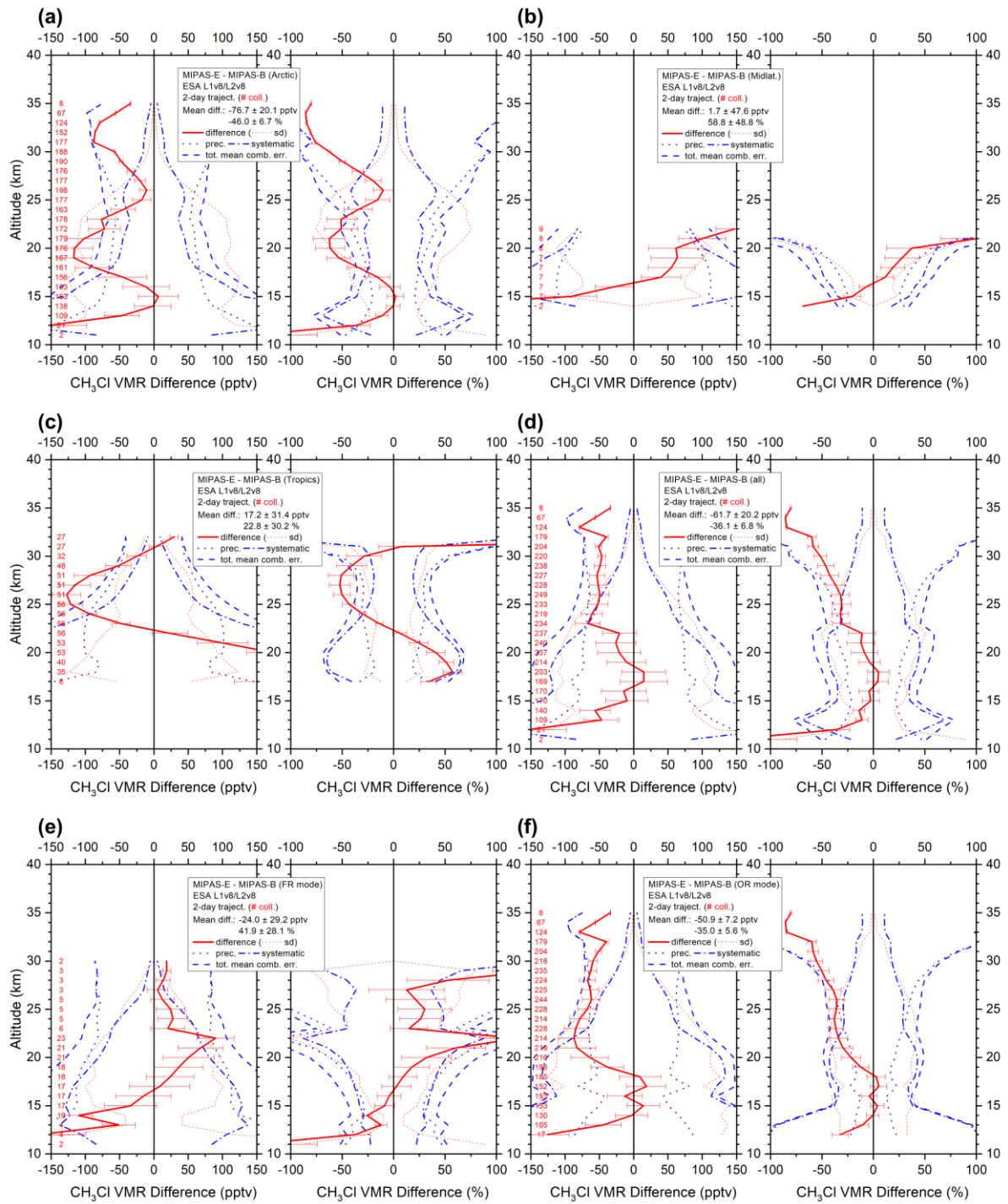


Figure 22. Same as Fig. 3 but for CH_3Cl .

580 **5 References**

- Bertaux, J. L., Mégie, G., Widemann, T., Chassefière, E., Pellinen, R., Kyrola, E., Korpela, S., and Simon, P.: Monitoring of ozone trend by stellar occultations: the GOMOS instrument, *Advances in Space Research*, 11, 237–242, [https://doi.org/10.1016/0273-1177\(91\)90426-K](https://doi.org/10.1016/0273-1177(91)90426-K), 1991.
- 585 Bovensmann, H., Burrows, J. P., Buchwitz, M., Frerick, J., Noël, S., Rozanov, V. V., Chance, K. V., and Goede, A. P. H.: *SCIAMACHY: Mission Objectives and Measurement Modes*, *J. Atmos. Sci.*, 56, 127–150, [https://doi.org/10.1175/1520-0469\(1999\)056<0127:SMOAMM>2.0.CO;2](https://doi.org/10.1175/1520-0469(1999)056<0127:SMOAMM>2.0.CO;2), 1999.
- Bracher, A., Sinnhuber, M., Rozanov, A., and Burrows, J. P.: Using a photochemical model
590 for the validation of NO₂ satellite measurements at different solar zenith angles, *Atmos. Chem. Phys.*, 5, 393–408, <https://doi.org/10.5194/acp-5-393-2005>, 2005.
- Brasseur, G. P. and Solomon, S.: *Aeronomy of the Middle Atmosphere: Chemistry and Physics of the Stratosphere and Mesosphere*, Third revised and enlarged edition, *Atmospheric and Oceanographic Sciences Library*, 32, Springer, Dordrecht, 2005.
- 595 Carpenter, L. J., Reimann, S., Burkholder, J. B., Clerbaux, C., Hall, B. D., Hossaini, R., Laube, J. C., and Yvon-Lewis, S. A.: Chapter 1: Update on Ozone-Depleting Substances (ODSs) and Other Gases of Interest to the Montreal Protocol, in: *Scientific Assessment of Ozone Depletion*, edited by: Ennis Christine A., World Meteorological Organization (WMO), 21–125, 2014.
- 600 Chirkov, M., Stiller, G. P., Laeng, A., Kellmann, S., von Clarmann, T., Boone, C. D., Elkins, J. W., Engel, A., Glatthor, N., Grabowski, U., Harth, C. M., Kiefer, M., Kolonjari, F., Krummel, P. B., Linden, A., Lunder, C. R., Miller, B. R., Montzka, S. A., Mühle, J., O'Doherty, S., Orphal, J., Prinn, R. G., Toon, G., Vollmer, M. K., Walker, K. A., Weiss, R. F., Wiecele, A., and Young, D.: Global HCFC-22 measurements with MIPAS:
605 retrieval, validation, global distribution and its evolution over 2005–2012, *Atmos. Chem. Phys.*, 16, 3345–3368, <https://doi.org/10.5194/acp-16-3345-2016>, 2016.
- Clarmann, T. von, Höpfner, M., Kellmann, S., Linden, A., Chauhan, S., Funke, B., Grabowski, U., Glatthor, N., Kiefer, M., Schieferdecker, T., Stiller, G. P., and Versick, S.: Retrieval of temperature, H₂O, O₃, HNO₃, CH₄, N₂O, ClONO₂ and ClO from MIPAS
610 reduced resolution nominal mode limb emission measurements, *Atmos. Meas. Tech.*, 2,

159–175, <https://doi.org/10.5194/amt-2-159-2009>, available at:

<https://amt.copernicus.org/articles/2/159/2009/>, 2009.

Clarmann, T. von and Johansson, S.: Chlorine nitrate in the atmosphere, *Atmos. Chem. Phys.*, 18, 15363–15386, <https://doi.org/10.5194/acp-18-15363-2018>, 2018.

615 Cortesi, U., Lambert, J. C., Clercq, C. de, Bianchini, G., Blumenstock, T., Bracher, A.,
Castelli, E., Catoire, V., Chance, K. V., Mazière, M. de, Demoulin, P., Godin-Beekmann,
S., Jones, N., Jucks, K., Keim, C., Kerzenmacher, T., Kuellmann, H., Kuttippurath, J.,
Iarlori, M., Liu, G. Y., Liu, Y., McDermid, I. S., Meijer, Y. J., Mencaraglia, F., Mikuteit,
S., Oelhaf, H., Piccolo, C., Pirre, M., Raspollini, P., Ravegnani, F., Reburn, W. J.,
620 Redaelli, G., Remedios, J. J., Sembhi, H., Smale, D., Steck, T., Taddei, A., Varotsos, C.,
Vigouroux, C., Waterfall, A., Wetzel, G., and Wood, S.: Geophysical validation of
MIPAS-ENVISAT operational ozone data, *Atmos. Chem. Phys.*, 7, 4807–4867,
<https://doi.org/10.5194/acp-7-4807-2007>, 2007.

Crutzen, P. J.: The possible importance of CSO for the sulfate layer of the stratosphere,
625 *Geophys. Res. Lett.*, 3, 73–76, <https://doi.org/10.1029/GL003i002p00073>, 1976.

Dessler, A. E., Schoeberl, M. R., Wang, T., Davis, S. M., Rosenlof, K. H., and Vernier, J.-P.:
Variations of stratospheric water vapor over the past three decades, *J. Geophys. Res.*
Atmos., 119, 12,588–12,598, <https://doi.org/10.1002/2014JD021712>, 2014.

Dhomse, S. S., Feng, W., Montzka, S. A., Hossaini, R., Keeble, J., Pyle, J. A., Daniel, J. S.,
630 and Chipperfield, M. P.: Delay in recovery of the Antarctic ozone hole from unexpected
CFC-11 emissions, *Nature Communications*, 10, 5781, <https://doi.org/10.1038/s41467-019-13717-x>, 2019.

Dinelli, B. M., Raspollini, P., Gai, M., Sgheri, L., Ridolfi, M., Ceccherini, S., Barbara, F.,
Zoppetti, N., Castelli, E., Papandrea, E., Pettinari, P., Dehn, A., Dudhia, A., Kiefer, M.,
635 Piro, A., Flaud, J.-M., López-Puertas, M., Moore, D., Remedios, J., and Bianchini, M.:
The ESA MIPAS/Envisat level2-v8 dataset: 10 years of measurements retrieved with
ORM v8.22, *Atmos. Meas. Tech.*, 14, 7975–7998, <https://doi.org/10.5194/amt-14-7975-2021>, 2021.

Dudhia, A., Jay, V. L., and Rodgers, C. D.: Microwindow selection for high-spectral-
640 resolution sounders, *Appl. Opt.*, 41, 3665, <https://doi.org/10.1364/AO.41.003665>, 2002.

- Engel, A., Bönisch, H., Schwarzenberger, T., Haase, H.-P., Grunow, K., Abalichin, J., and Sala, S.: Long-term validation of ESA operational retrieval (version 6.0) of MIPAS Envisat vertical profiles of methane, nitrous oxide, CFC11, and CFC12 using balloon-borne observations and trajectory matching, *Atmos. Meas. Tech.*, 9, 1051–1062, <https://doi.org/10.5194/amt-9-1051-2016>, 2016.
- 645
- ESA: New Envisat MIPAS L2 dataset reprocessed with ORM v822 available - Earth Online, available at: <https://earth.esa.int/eogateway/news/new-envisat-mipas-l2-dataset-reprocessed-with-orm-v822-available> (last access: 12 July 2022), 2021.
- ESA: ESA declares end of mission for Envisat, available at:
- 650 https://www.esa.int/Applications/Observing_the_Earth/Envisat/ESA_declares_end_of_mission_for_Envisat (last access: 12 July 2022), 2012.
- Fischer, H., Birk, M., Blom, C., Carli, B., Carlotti, M., Clarmann, T. von, Delbouille, L., Dudhia, A., Ehhalt, D., Endemann, M., Flaud, J. M., Gessner, R., Kleinert, A., Koopman, R., Langen, J., López-Puertas, M., Mosner, P., Nett, H., Oelhaf, H., Perron, G., Remedios, J., Ridolfi, M., Stiller, G., and Zander, R.: MIPAS: an instrument for atmospheric and climate research, *Atmos. Chem. Phys.*, 8, 2151–2188, <https://doi.org/10.5194/acp-8-2151-2008>, 2008.
- 655
- Friedl-Vallon, F., Maucher, G., Seefeldner, M., Trieschmann, O., Kleinert, A., Lengel, A., Keim, C., Oelhaf, H., and Fischer, H.: Design and characterization of the balloon-borne Michelson Interferometer for Passive Atmospheric Sounding (MIPAS-B2), *Appl. Opt.*, 43, 3335, <https://doi.org/10.1364/AO.43.003335>, 2004.
- 660
- Fu, D., Boone, C. D., Bernath, P. F., Walker, K. A., Nassar, R., Manney, G. L., and McLeod, S. D.: Global phosgene observations from the Atmospheric Chemistry Experiment (ACE) mission, *Geophys. Res. Lett.*, 34, 32, <https://doi.org/10.1029/2007GL029942>, 2007.
- 665
- Glatthor, N., Clarmann, T. von, Stiller, G. P., Funke, B., Koukouli, M. E., Fischer, H., Grabowski, U., Höpfner, M., Kellmann, S., and Linden, A.: Large-scale upper tropospheric pollution observed by MIPAS HCN and C₂H₆ global distributions, *Atmos. Chem. Phys.*, 9, 9619–9634, <https://doi.org/10.5194/acp-9-9619-2009>, 2009.
- 670
- Glatthor, N., Höpfner, M., Leyser, A., Stiller, G. P., Clarmann, T. von, Grabowski, U., Kellmann, S., Linden, A., Sinnhuber, B.-M., Krysztofiak, G., and Walker, K. A.: Global

carbonyl sulfide (OCS) measured by MIPAS/Envisat during 2002–2012, *Atmos. Chem. Phys.*, 17, 2631–2652, <https://doi.org/10.5194/acp-17-2631-2017>, 2017.

675 Grunow, K.: Anwendung von Trajektorien zur ENVISAT-Validierung und zur Untersuchung der Luftmassenherkunft in der Stratosphäre, PhD, Free University Berlin, Berlin, Germany, 2009.

Harrison, J. J.: New and improved infrared absorption cross sections for dichlorodifluoromethane (CFC-12), *Atmos. Meas. Tech.*, 8, 3197–3207, <https://doi.org/10.5194/amt-8-3197-2015>, 2015.

680 Harrison, J. J., Chipperfield, M. P., Dudhia, A., Cai, S., Dhomse, S., Boone, C. D., and Bernath, P. F.: Satellite observations of stratospheric carbonyl fluoride, *Atmos. Chem. Phys.*, 14, 11915–11933, <https://doi.org/10.5194/acp-14-11915-2014>, 2014.

Harrison, J. J.: New and improved infrared absorption cross sections for chlorodifluoromethane (HCFC-22), *Atmos. Meas. Tech.*, 9, 2593–2601, <https://doi.org/10.5194/amt-9-2593-2016>, 2016.

685 Harrison, J. J., Boone, C. D., and Bernath, P. F.: New and improved infra-red absorption cross sections and ACE-FTS retrievals of carbon tetrachloride (CCl₄), *Journal of Quantitative Spectroscopy and Radiative Transfer*, 186, 139–149, <https://doi.org/10.1016/j.jqsrt.2016.04.025>, 2017.

690 Hegglin, M. I., Tegtmeier, S., Anderson, J., Bourassa, A. E., Brohede, S., Degenstein, D., Froidevaux, L., Funke, B., Gille, J., Kasai, Y., Kyrölä, E. T., Lumpe, J., Murtagh, D., Neu, J. L., Pérot, K., Remsberg, E. E., Rozanov, A., Toohey, M., Urban, J., Clarmann, T. von, Walker, K. A., Wang, H.-J., Arosio, C., Damadeo, R., Fuller, R. A., Lingenfelter, G., McLinden, C., Pendlebury, D., Roth, C., Ryan, N. J., Sioris, C., Smith, L., and Weigel, K.: Overview and update of the SPARC Data Initiative: comparison of stratospheric
695 composition measurements from satellite limb sounders, *Earth Syst. Sci. Data*, 13, 1855–1903, <https://doi.org/10.5194/essd-13-1855-2021>, 2021.

Höpfner, M., Oelhaf, H., Wetzel, G., Friedl-Vallon, F., Kleinert, A., Lengel, A., Maucher, G., Nordmeyer, H., Glatthor, N., Stiller, G., Clarmann, T. v., Fischer, H., Kröger, C., and Deshler, T.: Evidence of scattering of tropospheric radiation by PSCs in mid-IR limb
700 emission spectra: MIPAS-B observations and KOPRA simulations, *Geophys. Res. Lett.*, 29, 119-1-119-4, <https://doi.org/10.1029/2001GL014443>, 2002.

- Hubert, D., Keppens, A., Granville, J., and Lambert, J.-C.: Validation report: comparison of MIPAS ORM 8.22 to ground-based data TN-BIRA-IASB-MultiTASTE-Phase-F-MIPAS-ORM8-Iss1-RevB, available at:
- 705 <https://earth.esa.int/eogateway/documents/20142/37627/TN-BIRA-IASB-MultiTASTE-Phase-F-MIPAS-ORM8-Iss1-RevB.pdf> (last access: 12 July 2022), 2020.
- Khosrawi, F., Lossow, S., Stiller, G. P., Rosenlof, K. H., Urban, J., Burrows, J. P., Damadeo, R. P., Eriksson, P., García-Comas, M., Gille, J. C., Kasai, Y., Kiefer, M., Nedoluha, G. E., Noël, S., Raspollini, P., Read, W. G., Rozanov, A., Sioris, C. E., Walker, K. A., and
- 710 Weigel, K.: The SPARC water vapour assessment II: comparison of stratospheric and lower mesospheric water vapour time series observed from satellites, *Atmos. Meas. Tech.*, 11, 4435–4463, <https://doi.org/10.5194/amt-11-4435-2018>, 2018.
- Kindler, T. P., Chameides, W. L., Wine, P. H., Cunnold, D. M., Alyea, F. N., and Franklin, J. A.: The fate of atmospheric phosgene and the stratospheric chlorine loadings of its parent
- 715 compounds: CCl₄, C₂Cl₄, C₂HCl₃, CH₃CCl₃, and CHCl₃, *J. Geophys. Res.*, 100, 1235–1251, <https://doi.org/10.1029/94JD02518>, 1995.
- Ko, M. K. W. and Dak Sze, N.: A 2-D model calculation of atmospheric lifetimes for N₂O, CFC-11 and CFC-12, *Nature*, 297, 317–319, <https://doi.org/10.1038/297317a0>, 1982.
- Kremser, S., Thomason, L. W., Hobe, M. von, Hermann, M., Deshler, T., Timmreck, C.,
- 720 Toohey, M., Stenke, A., Schwarz, J. P., Weigel, R., Fueglistaler, S., Prata, F. J., Vernier, J.-P., Schlager, H., Barnes, J. E., Antuña-Marrero, J.-C., Fairlie, D., Palm, M., Mahieu, E., Notholt, J., Rex, M., Bingen, C., Vanhellemont, F., Bourassa, A., Plane, J. M. C., Klocke, D., Carn, S. A., Clarisse, L., Trickl, T., Neely, R., James, A. D., Rieger, L., Wilson, J. C., and Meland, B.: Stratospheric aerosol-Observations, processes, and impact on climate,
- 725 *Rev. Geophys.*, 54, 278–335, <https://doi.org/10.1002/2015RG000511>, 2016.
- Li, Q., Jacob, D. J., Yantosca, R. M., Heald, C. L., Singh, H. B., Koike, M., Zhao, Y., Sachse, G. W., and Streets, D. G.: A global three-dimensional model analysis of the atmospheric budgets of HCN and CH₃CN: Constraints from aircraft and ground measurements, *J. Geophys. Res.*, 108, 955, <https://doi.org/10.1029/2002JD003075>, 2003.
- 730 Lossow, S., Khosrawi, F., Kiefer, M., Walker, K. A., Bertaux, J.-L., Blanot, L., Russell, J. M., Remsberg, E. E., Gille, J. C., Sugita, T., Sioris, C. E., Dinelli, B. M., Papandrea, E., Raspollini, P., García-Comas, M., Stiller, G. P., Clarmann, T. von, Dudhia, A., Read, W.

- G., Nedoluha, G. E., Damadeo, R. P., Zawodny, J. M., Weigel, K., Rozanov, A., Azam, F., Bramstedt, K., Noël, S., Burrows, J. P., Sagawa, H., Kasai, Y., Urban, J., Eriksson, P.,
735 Murtagh, D. P., Hervig, M. E., Högberg, C., Hurst, D. F., and Rosenlof, K. H.: The SPARC water vapour assessment II: profile-to-profile comparisons of stratospheric and lower mesospheric water vapour data sets obtained from satellites, *Atmos. Meas. Tech.*, 12, 2693–2732, <https://doi.org/10.5194/amt-12-2693-2019>, 2019.
- Lossow, S., Hurst, D. F., Rosenlof, K. H., Stiller, G. P., Clarmann, T. von, Brinkop, S.,
740 Dameris, M., Jöckel, P., Kinnison, D. E., Plieninger, J., Plummer, D. A., Ploeger, F., Read, W. G., Remsberg, E. E., Russell, J. M., and Tao, M.: Trend differences in lower stratospheric water vapour between Boulder and the zonal mean and their role in understanding fundamental observational discrepancies, *Atmos. Chem. Phys.*, 18, 8331–8351, <https://doi.org/10.5194/acp-18-8331-2018>, 2018.
- 745 Manney, G. L., Michelsen, H. A., Bevilacqua, R. M., Gunson, M. R., Irion, F. W., Livesey, N. J., Oberheide, J., Riese, M., Russell, J. M., Toon, G. C., and Zawodny, J. M.: Comparison of satellite ozone observations in coincident air masses in early November 1994, *J. Geophys. Res.*, 106, 9923–9943, 2001.
- Michelsen, H. A., Manney, G. L., Gunson, M. R., and Zander, R.: Correlations of
750 stratospheric abundances of NO_y, O₃, N₂O, and CH₄ derived from ATMOS measurements, *J. Geophys. Res. Atmos.*, 103, 28347–28359, <https://doi.org/10.1029/98JD02850>, 1998.
- Naujokat, B. and Grunow, K.: The stratospheric Arctic winter 2002/03: Balloon flight planning by trajectory calculations, 16th Esa Symposium on European Rocket and Balloon Programmes and Related Research, Proceedings, 530, 421–425, 2003.
- 755 Parker, R. J., Remedios, J. J., Moore, D. P., and Kanawade, V. P.: Acetylene C₂H₂ retrievals from MIPAS data and regions of enhanced upper tropospheric concentrations in August 2003, *Atmos. Chem. Phys.*, 11, 10243–10257, <https://doi.org/10.5194/acp-11-10243-2011>, 2011.
- Payan, S., Camy-Peyret, C., Oelhaf, H., Wetzell, G., Maucher, G., Keim, C., Pirre, M., Huret,
760 N., Engel, A., Volk, M. C., Kuellmann, H., Kuttippurath, J., Cortesi, U., Bianchini, G., Mencaraglia, F., Raspollini, P., Redaelli, G., Vigouroux, C., Mazière, M. de, Mikuteit, S., Blumenstock, T., Velazco, V., Notholt, J., Mahieu, E., Duchatelet, P., Smale, D., Wood, S., Jones, N., Piccolo, C., Payne, V., Bracher, A., Glatthor, N., Stiller, G., Grunow, K.,

- 765 Jeseck, P., Te, Y., and Butz, A.: Validation of version-4.61 methane and nitrous oxide
observed by MIPAS, *Atmos. Chem. Phys.*, 9, 413–442, [https://doi.org/10.5194/acp-9-413-](https://doi.org/10.5194/acp-9-413-2009)
2009, 2009.
- Pettinari, P., Barbara, F., Ceccherini, S., Dinelli, B. M., Gai, M., Raspollini, P., Sgheri, L.,
Valeri, M., Wetzels, G., Zoppetti, N., and Ridolfi, M.: Phosgene distribution derived from
MIPAS ESA v8 data: intercomparisons and trends, *Atmos. Meas. Tech.*, 14, 7959–7974,
770 <https://doi.org/10.5194/amt-14-7959-2021>, 2021.
- Phillips, D. L.: A technique for the numerical solution of certain integral equations of the first
kind, *J. Assoc. Comput. Math.*, 9, 84–97, <https://doi.org/10.1145/321105.321114>, 1962.
- Prinn, R. G., Weiss, R. F., Fraser, P. J., Simmonds, P. G., Cunnold, D. M., Alyea, F. N.,
O'Doherty, S., Salameh, P., Miller, B. R., Huang, J., Wang, R. H. J., Hartley, D. E., Harth,
775 C., Steele, L. P., Sturrock, G., Midgley, P. M., and McCulloch, A.: A history of
chemically and radiatively important gases in air deduced from ALE/GAGE/AGAGE, *J.*
Geophys. Res., 105, 17751–17792, <https://doi.org/10.1029/2000JD900141>, 2000.
- Raspollini, P., Arnone, E., Barbara, F., Bianchini, M., Carli, B., Ceccherini, S., Chipperfield,
M. P., Dehn, A., Della Fera, S., Dinelli, B. M., Dudhia, A., Flaud, J.-M., Gai, M., Kiefer,
780 M., López-Puertas, M., Moore, D. P., Piro, A., Remedios, J. J., Ridolfi, M., Sembhi, H.,
Sgheri, L., and Zoppetti, N.: Level 2 processor and auxiliary data for ESA Version 8 final
full mission analysis of MIPAS measurements on ENVISAT, *Atmos. Meas. Tech.*, 15,
1871–1901, <https://doi.org/10.5194/amt-15-1871-2022>, 2022.
- Raspollini, P., Piro, A., Hubert, D., Keppens, A., Lambert, J.-C., Wetzels, G., Moore, D.,
785 Ceccherini, S., Gai, M., Barbara, F., and Zoppetti, N.: Environmental Satellite
(ENVISAT) Michelson Interferometer for Passive Atmospheric Sounding (MIPAS), ESA
Level 2 version 8.22 products - product quality readme file, available at:
[https://earth.esa.int/eogateway/documents/20142/37627/README_V8_issue_1.0_202012](https://earth.esa.int/eogateway/documents/20142/37627/README_V8_issue_1.0_20201221.pdf)
21.pdf (last access: 12 July 2022), 2020.
- 790 Raspollini, P., Carli, B., Carlotti, M., Ceccherini, S., Dehn, A., Dinelli, B. M., Dudhia, A.,
Flaud, J.-M., López-Puertas, M., Niro, F., Remedios, J. J., Ridolfi, M., Sembhi, H., Sgheri,
L., and Clarmann, T. von: Ten years of MIPAS measurements with ESA Level 2
processor V6 – Part 1: Retrieval algorithm and diagnostics of the products, *Atmos. Meas.*
Tech., 6, 2419–2439, <https://doi.org/10.5194/amt-6-2419-2013>, 2013.

- 795 Raspollini, P., Belotti, C., Burgess, A., Carli, B., Carlotti, M., Ceccherini, S., Dinelli, B. M.,
Dudhia, A., Flaud, J.-M., Funke, B., Höpfner, M., Lopez-Puertas, M., Payne, V., Piccolo,
C., Remedios, J. J., Ridolfi, M., and Spang, R.: MIPAS level 2 operational analysis,
Atmos. Chem. Phys., 6, 5605–5630, <https://doi.org/10.5194/acp-6-5605-2006>, 2006.
- 800 Renard, J.-B., Berthet, G., Brogniez, C., Catoire, V., Fussen, D., Goutail, F., Oelhaf, H.,
Pommereau, J.-P., Roscoe, H. K., Wetzels, G., Chartier, M., Robert, C., Balois, J.-Y.,
Verwaerde, C., Auriol, F., François, P., Gaubicher, B., and Wursteisen, P.: Validation of
GOMOS-Envisat vertical profiles of O₃ NO₂ NO₃ and aerosol extinction using balloon-
borne instruments and analysis of the retrievals, *J. Geophys. Res.*, 113, n/a-n/a,
<https://doi.org/10.1029/2007JA012345>, 2008.
- 805 Ridolfi, M., Blum, U., Carli, B., Catoire, V., Ceccherini, S., Claude, H., Clercq, C. de, Fricke,
K. H., Friedl-Vallon, F., Iarlori, M., Keckhut, P., Kerridge, B., Lambert, J.-C., Meijer, Y.
J., Mona, L., Oelhaf, H., Pappalardo, G., Pirre, M., Rizi, V., Robert, C., Swart, D.,
Clarmann, T. von, Waterfall, A., and Wetzels, G.: Geophysical validation of temperature
810 measurements, *Atmos. Chem. Phys.*, 7, 4459–4487, <https://doi.org/10.5194/acp-7-4459-2007>, 2007.
- Ridolfi, M., Carli, B., Carlotti, M., Clarmann, T. von, Dinelli, B. M., Dudhia, A., Flaud, J.-M.,
Höpfner, M., Morris, P. E., Raspollini, P., Stiller, G., and Wells, R. J.: Optimized forward
model and retrieval scheme for MIPAS near-real-time data processing, *Appl. Opt.*, 39,
815 1323, <https://doi.org/10.1364/AO.39.001323>, 2000.
- Rodgers, C. D.: *Inverse methods for atmospheric sounding*, 2, World Sci., 2000.
- Rothman, L. S., Gordon, I. E., Barbe, A., Benner, D., Bernath, P. F., Birk, M., Boudon, V.,
Brown, L. R., Campargue, A., Champion, J.-P., Chance, K., Coudert, L. H., Dana, V.,
Devi, V. M., Fally, S., Flaud, J.-M., Gamache, R. R., Goldman, A., Jacquemart, D.,
820 Kleiner, I., Lacome, N., Lafferty, W. J., Mandin, J.-Y., Massie, S. T., Mikhailenko, S. N.,
Miller, C. E., Moazzen-Ahmadi, N., Naumenko, O. V., Nikitin, A. V., Orphal, J.,
Perevalov, V. I., Perrin, A., Predoi-Cross, A., Rinsland, C. P., Rotger, M., Šimečková, M.,
Smith, M., Sung, K., Tashkun, S. A., Tennyson, J., Toth, R. A., Vandaele, A. C., and
Vander Auwera, J.: The HITRAN 2008 molecular spectroscopic database, *Journal of*
825 *Quantitative Spectroscopy and Radiative Transfer*, 110, 533–572,
<https://doi.org/10.1016/j.jqsrt.2009.02.013>, 2009.

- Rudolph, J.: The tropospheric distribution and budget of ethane, *J. Geophys. Res.*, 100, 11369, <https://doi.org/10.1029/95JD00693>, 1995.
- 830 Sagawa, H., Sato, T. O., Baron, P., Dupuy, E., Livesey, N., Urban, J., Clarmann, T. von, Lange, A. de, Wetzel, G., Connor, B. J., Kagawa, A., Murtagh, D., and Kasai, Y.: Comparison of SMILES ClO profiles with satellite, balloon-borne and ground-based measurements, *Atmos. Meas. Tech.*, 6, 3325–3347, <https://doi.org/10.5194/amt-6-3325-2013>, 2013.
- 835 Singh, H. B., Herlth, D., Kolyer, R., Chatfield, R., Viezee, W., Salas, L. J., Chen, Y., Bradshaw, J. D., Sandholm, S. T., Talbot, R., Gregory, G. L., Anderson, B., Sachse, G. W., Browell, E., Bachmeier, A. S., Blake, D. R., Heikes, B., Jacob, D., and Fuelberg, H. E.: Impact of biomass burning emissions on the composition of the South Atlantic troposphere: Reactive nitrogen and ozone, *J. Geophys. Res.*, 101, 24203–24219, <https://doi.org/10.1029/96JD01018>, 1996.
- 840 Sinnhuber, M., Burrows, J. P., Chipperfield, M. P., Jackman, C. H., Kallenrode, M.-B., Künzi, K. F., and Quack, M.: A model study of the impact of magnetic field structure on atmospheric composition during solar proton events, *Geophys. Res. Lett.*, 30, 1781, <https://doi.org/10.1029/2003GL017265>, 2003.
- 845 SPARC: The SPARC Data Initiative: Assessment of stratospheric trace gas and aerosol climatologies from satellite limb sounders. By M. I. Hegglin and S. Tegtmeier (eds.), SPARC Report No. 8, WCRP-5/2017, available at: <https://www.sparc-climate.org/publications/sparc-reports/> (last access: 22 September 2022), 2017.
- 850 Stiller, G. P., Clarmann, T. von, Funke, B., Glatthor, N., Hase, F., Höpfner, M., and Linden, A.: Sensitivity of trace gas abundances retrievals from infrared limb emission spectra to simplifying approximations in radiative transfer modelling, *Journal of Quantitative Spectroscopy and Radiative Transfer*, 72, 249–280, [https://doi.org/10.1016/S0022-4073\(01\)00123-6](https://doi.org/10.1016/S0022-4073(01)00123-6), 2002.
- 855 Tchana, F. K., Lafferty, W. J., Flaud, J.-M., Manceron, L., and Ndao, M.: High-resolution analysis of the ν_1 and ν_5 bands of phosgene $^{35}\text{Cl}_2\text{CO}$ and $^{35}\text{Cl}^{37}\text{ClCO}$, *Molecular Physics*, 113, 3241–3246, <https://doi.org/10.1080/00268976.2015.1015638>, 2015.
- Tikhonov, A. N.: On the solution of ill-posed problems and the method of regularization, *Dokl. Acad. Nauk SSSR*, 151, 501–504, 1963.

- Toon, G. C., Blavier, J.-F., Sen, B., and Drouin, B. J.: Atmospheric COCl₂ measured by solar occultation spectrometry, *Geophys. Res. Lett.*, 28, 2835–2838, <https://doi.org/10.1029/2000GL012156>, 2001.
- 860 Valeri, M., Barbara, F., Boone, C., Ceccherini, S., Gai, M., Maucher, G., Raspollini, P., Ridolfi, M., Sgheri, L., Wetzel, G., and Zoppetti, N.: CCl₄ distribution derived from MIPAS ESA v7 data: intercomparisons, trend, and lifetime estimation, *Atmos. Chem. Phys.*, 17, 10143–10162, <https://doi.org/10.5194/acp-17-10143-2017>, 2017.
- 865 Valeri, M., Carlotti, M., Flaud, J.-M., Raspollini, P., Ridolfi, M., and Dinelli, B. M.: Phosgene in the UTLS: seasonal and latitudinal variations from MIPAS observations, *Atmos. Meas. Tech.*, 9, 4655–4663, <https://doi.org/10.5194/amt-9-4655-2016>, 2016.
- 870 Wang, D. Y., Höpfner, M., Blom, C. E., Ward, W. E., Fischer, H., Blumenstock, T., Hase, F., Keim, C., Liu, G. Y., Mikuteit, S., Oelhaf, H., Wetzel, G., Cortesi, U., Mencaraglia, F., Bianchini, G., Redaelli, G., Pirre, M., Catoire, V., Huret, N., Vigouroux, C., Mazière, M. de, Mahieu, E., Demoulin, P., Wood, S., Smale, D., Jones, N., Nakajima, H., Sugita, T., Urban, J., Murtagh, D., Boone, C. D., Bernath, P. F., Walker, K. A., Kuttippurath, J., Kleinböhl, A., Toon, G., and Piccolo, C.: Validation of MIPAS HNO₃ operational data, *Atmos. Chem. Phys.*, 7, 4905–4934, <https://doi.org/10.5194/acp-7-4905-2007>, 2007.
- 875 Wetzel, G., Höpfner, M., and Oelhaf, H.: CCN #2: Support to MIPAS level 2 processor verification and validation - Phase F: Report to MS6_2: L1v8/L2v8 FM comparison for GL1-GL3; Long-term validation of MIPAS ESA operational products using MIPAS-B measurements, available at: https://earth.esa.int/eogateway/documents/20142/37627/kit_ccn_2_esa_tn-fr_2020_01.pdf (last access: 12 July 2022), 2020.
- 880 Wetzel, G., Oelhaf, H., Birk, M., Lange, A. de, Engel, A., Friedl-Vallon, F., Kirner, O., Kleinert, A., Maucher, G., Nordmeyer, H., Orphal, J., Ruhnke, R., Sinnhuber, B.-M., and Vogt, P.: Partitioning and budget of inorganic and organic chlorine species observed by MIPAS-B and TELIS in the Arctic in March 2011, *Atmos. Chem. Phys.*, 15, 8065–8076, <https://doi.org/10.5194/acp-15-8065-2015>, 2015.
- 885 Wetzel, G., Oelhaf, H., Berthet, G., Bracher, A., Cornacchia, C., Feist, D. G., Fischer, H., Fix, A., Iarlori, M., Kleinert, A., Lengel, A., Milz, M., Mona, L., Müller, S. C., Ovarlez, J., Pappalardo, G., Piccolo, C., Raspollini, P., Renard, J.-B., Rizi, V., Rohs, S., Schiller, C.,

- 890 Stiller, G., Weber, M., and Zhang, G.: Validation of MIPAS-ENVISAT H₂O operational data collected between July 2002 and March 2004, *Atmos. Chem. Phys.*, 13, 5791–5811, <https://doi.org/10.5194/acp-13-5791-2013>, 2013a.
- Wetzel, G., Oelhaf, H., Friedl-Vallon, F., Kleinert, A., Maucher, G., Nordmeyer, H., and Orphal, J.: Long-term intercomparison of MIPAS additional species ClONO₂, N₂O₅, CFC-11, and CFC-12 with MIPAS-B measurements, *Annals of Geophysics*, 56, 895 <https://doi.org/10.4401/ag-6329>, 2013b.
- Wetzel, G., Oelhaf, H., Kirner, O., Friedl-Vallon, F., Ruhnke, R., Ebersoldt, A., Kleinert, A., Maucher, G., Nordmeyer, H., and Orphal, J.: Diurnal variations of reactive chlorine and nitrogen oxides observed by MIPAS-B inside the January 2010 Arctic vortex, *Atmos. Chem. Phys.*, 12, 6581–6592, <https://doi.org/10.5194/acp-12-6581-2012>, 2012.
- 900 Wetzel, G., Oelhaf, H., Kirner, O., Ruhnke, R., Friedl-Vallon, F., Kleinert, A., Maucher, G., Fischer, H., Birk, M., Wagner, G., and Engel, A.: First remote sensing measurements of ClOOCl along with ClO and ClONO₂ in activated and deactivated Arctic vortex conditions using new ClOOCl IR absorption cross sections, *Atmos. Chem. Phys.*, 10, 931–945, <https://doi.org/10.5194/acp-10-931-2010>, 2010.
- 905 Wetzel, G., Sugita, T., Nakajima, H., Tanaka, T., Yokota, T., Friedl-Vallon, F., Kleinert, A., Maucher, G., and Oelhaf, H.: Technical Note: Intercomparison of ILAS-II version 2 and 1.4 trace species with MIPAS-B measurements, *Atmos. Chem. Phys.*, 8, 1119–1126, <https://doi.org/10.5194/acp-8-1119-2008>, 2008.
- Wetzel, G., Bracher, A., Funke, B., Goutail, F., Hendrick, F., Lambert, J.-C., Mikuteit, S., 910 Piccolo, C., Pirre, M., Bazureau, A., Belotti, C., Blumenstock, T., Mazière, M. de, Fischer, H., Huret, N., Ionov, D., López-Puertas, M., Maucher, G., Oelhaf, H., Pommereau, J.-P., Ruhnke, R., Sinnhuber, M., Stiller, G., van Roozendaal, M., and Zhang, G.: Validation of MIPAS-ENVISAT NO₂ operational data, *Atmos. Chem. Phys.*, 7, 3261–3284, <https://doi.org/10.5194/acp-7-3261-2007>, 2007.
- 915 Wetzel, G., Oelhaf, H., Friedl-Vallon, F., Kleinert, A., Lengel, A., Maucher, G., Nordmeyer, H., Ruhnke, R., Nakajima, H., Sasano, Y., Sugita, T., and Yokota, T.: Intercomparison and validation of ILAS-II version 1.4 target parameters with MIPAS-B measurements, *J. Geophys. Res.*, 111, 281, <https://doi.org/10.1029/2005JD006287>, 2006.

- 920 Wiegele, A., Glatthor, N., Höpfner, M., Grabowski, U., Kellmann, S., Linden, A., Stiller, G.,
and Clarmann, T. von: Global distributions of C₂H₆, C₂H₂, HCN, and PAN retrieved from
MIPAS reduced spectral resolution measurements, *Atmos. Meas. Tech.*, 5, 723–734,
<https://doi.org/10.5194/amt-5-723-2012>, 2012.
- 925 Xiao, Y., Logan, J. A., Jacob, D. J., Hudman, R. C., Yantosca, R., and Blake, D. R.: Global
budget of ethane and regional constraints on U.S. sources, *J. Geophys. Res.*, 113, 955,
<https://doi.org/10.1029/2007JD009415>, 2008.
- Yokouchi, Y., Noijiri, Y., Barrie, L. A., Toom-Sauntry, D., Machida, T., Inuzuka, Y.,
Akimoto, H., Li, H. J., Fujinuma, Y., and Aoki, S.: A strong source of methyl chloride to
the atmosphere from tropical coastal land, *Nature*, 403, 295–298,
<https://doi.org/10.1038/35002049>, 2000.
- 930 Zhang, G., Wetzell, G., Oelhaf, H., Friedl-Vallon, F., Kleinert, A., Lengl, A., Maucher, G.,
Nordmeyer, H., Grunow, K., and Fischer, H.: Validation of atmospheric chemistry
measurements from MIPAS, SCIAMACHY, GOMOS onboard ENVISAT by
observations of balloon-borne MIPAS-B, *Sci. China Earth Sci.*, 53, 1533–1541,
<https://doi.org/10.1007/s11430-010-3059-3>, 2010.

935